# Line intensities of 12C2H2 in the 7.7 $\mu$m spectral region

Laura Gomez, David Jacquemart, Nelly Lacome, Jean-Yves Mandin

# Line intensities of $^{12}C_2H_2$ in the 7.7 µm spectral region

L. Gomez [a,b], D. Jacquemart [a,b,*], N. Lacome [a,b], J.-Y. Mandin [c,d]

[a] *UPMC Univ Paris 06, UMR 7075, Laboratoire de Dynamique Interactions et Réactivité, Case courrier 49, Bât. F 74, 4, place Jussieu, 75252 Paris Cedex 05, France*

[b] *CNRS, UMR 7075, Laboratoire de Dynamique Interactions et Réactivité, Case courrier 49, Bât. F 74, 4, place Jussieu, 75252 Paris Cedex 05, France*

[c] *UPMC Univ Paris 06, UMR 7092, Laboratoire de Physique Moléculaire pour l'Atmosphère et l'Astrophysique, Case courrier 76, 4, place Jussieu, 75252 Paris Cedex 05, France*

[d] *CNRS, UMR 7092, Laboratoire de Physique Moléculaire pour l'Atmosphère et l'Astrophysique, Case courrier 76, 4, place Jussieu, 75252 Paris Cedex 05, France*

Received 2009

* Corresponding author. Tel.: + 33-1-44-27-36-82; fax: + 33-1-44-27-30-21.
*E-mail address*: david.jacquemart@upmc.fr (D. Jacquemart).

**Abstract**

Absolute intensities of 414 lines are measured in eight bands of the 7.7 μm spectral region of the $^{12}C_2H_2$ molecule, with an average accuracy of 5%. Vibrational transition dipole moment squared values and empirical Herman-Wallis coefficients are obtained in order to model the rotational dependence of the transition dipole moment squared, except for some forbidden bands for which smoothed values are given. These data are used to calculate a line list for atmospheric or astrophysical applications.

*Keywords:* Acetylene; Infrared; Vibro-rotational transitions; Line intensities; Databases

## 1. Introduction

The 7.7 µm spectral region of acetylene $^{12}C_2H_2$ corresponds to the $\Delta P = 2$ sequence of vibrational transitions [1], $P$ being a pseudo-quantum number equals to $5v_1 + 3v_2 + 5v_3 + v_4 + v_5$, where $v_1$, $v_2$, $v_3$, $v_4$, and $v_5$ are the quantum numbers associated with the normal modes of vibration of the molecule in the ground electronic state. The more extensive work on this spectral region is this of Kabbadj et al [2] who assigned vibro-rotational lines in 16 bands around the $(\nu_4 + \nu_5)^0_+$ strong cold band at 1328 cm$^{-1}$. These 16 bands are hot bands, except for $(\nu_4 + \nu_5)^2$ at 1343 cm$^{-1}$. Among them, four "forbidden" bands were observed by Kabbadj et al, i.e., two $\Delta \leftarrow \Sigma$ and one $\Sigma \leftarrow \Delta$ bands, as also one $\Phi \leftarrow \Pi$ band. Recently, Robert et al [3] performed a global vibration-rotation analysis on states up to 3000 cm$^{-1}$, thus including the 7.7 µm spectral region.

The integrated intensity of the band at 1328 cm$^{-1}$ was first measured by Kelly et al [4], and later more accurately by Varanasi and Bangaru [5], and by Koops et al [6]. Theoretical calculations of this band intensity was performed by Abbouti Temsamani et al [7]. Intensities of a few lines of the *R*-branch of $(\nu_4 + \nu_5)^0_+$ were obtained by Podolske et al [8]. A few years ago, an accurate set of absolute line intensities was obtained by Vander Auwera [9] for the cold bands $(\nu_4 + \nu_5)^0_+$ and $(\nu_4 + \nu_5)^2$, the accuracy being estimated better than 2%. Intensities of some lines of $(\nu_4 + \nu_5)^0_+$ were measured again by Jacquemart et al [10] and Lepère et al [11], confirming the announced accuracy. Furthermore, collisional widths of $(\nu_4 + \nu_5)^0_+$ were studied by Varanasi et al [12] ($N_2$-broadening at 153 and 200 K), then by Podolske et al [8] ($N_2$- and He-broadening at room temperature) and by Devi et al [13] ($N_2$- and air-broadening at room temperature), whereas self-broadening coefficients were obtained recently by Lepère et al [11], as well as some $N_2$-broadening coefficients by Fissiaux et al [14] and Dyne et al [15].

The aim of this work is to initiate absolute line intensity measurements in bands for which no result has been reported in the literature. Line intensities are known for the $(\nu_4 + \nu_5)^0_+$ and $(\nu_4 + \nu_5)^2$ bands [9], but they are unknown for the numerous other bands observed and assigned by Kabbadj et al [2]. These bands are gathered in Table 1. In this table, a given value of $P$ is assigned to a given set of interacting vibrational states, named polyad or cluster. Then, polyads are noted $\{P\nu_5\}$. Vibrational levels are noted $v_1\ v_2\ v_3\ (v_4\ v_5)^{\ell}_{\pm}\ r$, with $\ell = |\ell_4 + \ell_5|$, $\ell_t$ being the vibrational angular momentum quantum number associated with the degenerate bending mode $t$, $\pm$ being the symmetry type for $\Sigma$ vibrational states ($\ell = 0$), and $r$ a roman numeral indicating the rank of the level, by decreasing energy value ($r$ = I for the highest energy level), inside the set of states having the same vibrational symmetry, and coupled by $\ell$-type resonances.

Intensity measurements were undertaken because the knowledge of $C_2H_2$ line intensities in the 7.7 µm spectral region is important for several applications, especially for astrophysical ones. For example, the acetylene molecule has been observed in the circumstellar envelopes of carbon-rich stars. Using the Infrared Spectrograph (IRS) on board the Spitzer Space Telescope (SST), Matsuura et al [16] detected acetylene bands at 7 and 14 µm in carbon-rich asymptotic giant branch stars in the Large Magellanic Cloud. Around 7 µm, spectroscopic databases as HITRAN [17] and GEISA [18] only contain line positions and intensities that Vander Auwera calculated from his absolute measurements in the $(\nu_4 + \nu_5)^0_+$ band [9], for the rotational quantum number $J$ up to 35. But intensities measured in Ref. [9] for some lines of the $(\nu_4 + \nu_5)^2$ band are not reported in the databases. The temperature of interest for applications being around

500 K [16], the knowledge of intensities in the remaining hot bands is also important. In the quoted paper [16], Matsuura et al could not reproduce the shapes that they observed in their IRS-SST spectra around 7 μm because of the lack of data in databases.

The acetylene spectrum being very crowded around 1300 $cm^{-1}$, we first focused our work on 8 bands, that include the strongest allowed bands and the forbidden ones for their interest. To perform intensity measurements, several spectra have been recorded with a Fourier transform spectrometer. A set of 414 absolute line intensities have been obtained with an average accuracy of 5%. Section 2 of the paper will be devoted to the experimental conditions and to the measurements. The results and their analysis will be given in Section 3. The last section explains how we have proceeded to set up a line list for databases.

## 2. Experimental details and measurements

Six spectra have been recorded with the rapid scan Bruker IFS 120 HR interferometer of the LADIR (LAboratoire de Dynamique, Interactions et Réactivité, Paris). Experimental conditions are gathered in Table 2. This interferometer was equipped with a Globar source, Ge/KBr beam splitter, and a photovoltaic MCT (Mercury-Cadmium-Telluride) detector. An optical filter covering the spectral region between 800 to 2000 $cm^{-1}$ has been used. The whole optical path was under vacuum and a multipass cell of 1-m base length was used. The cell was equipped with KCl windows. The temperature of the gas in the cell was recorded via four platinum probes at different places inside the cell. The uncertainty on the temperature measurements has been estimated to be ±0.5 K. Pressures were measured using two full scale ranges MKS Baratrons (10- and 100-Torr manometers) with an accuracy of 0.5%. Each scan among about 400 recorded for every spectrum has then been individually transformed to a spectrum using the Fourier transform procedure included in the Bruker software OPUS package [19], selecting a Mertz phase error correction [20,21].

To deduce line intensities from the spectra, a multispectrum procedure was used following a method already described [22]. In this method, experimental data are concatenated in a single vector, and the adjusted parameters are constrained to be the same for all the spectra simultaneously adjusted. Then, line parameters are obtained in a single run of the procedure and their accuracy is improved. Before to run the procedure, one has first to adjust an effective value of the iris radius for each spectrum, to check that there is no residual due to a phase error, and to calibrate the absolute wavenumber scale of each spectrum. For that, the wavenumbers given by Vander Auwera around 7.7 μm [9] have been used. The accuracy of measured line positions of not too weak and well isolated lines is estimated to be 0.0002 $cm^{-1}$ on the mean. Then, the multispectrum procedure was run in the following conditions. A Voigt profile was used to calculate the absorption coefficient of the lines. The Doppler-width is kept fixed at its theoretical value and the baseline is adjusted as a polynomial of the second degree around each studied line. Because of the relatively low pressures, the self-broadening coefficients were fixed at the values calculated according to Ref. [23], and the self-shifting coefficients were fixed at zero. On the whole, 414 line intensities have been measured in 8 bands with an average accuracy estimated around 5%, but that can be degraded up to 10% for very weak lines or overlapped ones. The results obtained for selected bands are given in Tables 3 and 4. Results obtained for the other bands can be found in the supplementary material attached to this paper.

## 3. Data reduction and results

For each line intensity $S(T_0)$ obtained from the multispectrum fitting procedure, in cm molecule$^{-1}$ for pure $^{12}C_2H_2$ (i.e., for a sample containing 100% of $^{12}C_2H_2$) at the standard temperature $T_0$ = 296 K, we used the following formula to deduce the transition dipole moment squared $|R|^2$, in D$^2$ (1 debye = $3.33546 \times 10^{-30}$ C m)

$$S(T_0) = (1/4\pi\varepsilon_0)\,(8\pi^3/3hc)\,[g''\nu_0 \;/\; g_V \;\; Q(T_0)]\,|R|^2\,L(J,\ell)\,\exp(-hcE''/kT_0)\,[1-\exp(-hc\nu_0/kT_0)], \quad (1)$$

where $1/4\pi\varepsilon_0 = 10^{-36}$ erg cm$^3$ D$^{-2}$; $h$ is Planck's constant equal to $6.6260755 \times 10^{-27}$ erg s (1 erg = $10^{-7}$ J); $c$ is the speed of light in vacuum equal to $2.99792458 \times 10^{10}$ cm s$^{-1}$; $g''$ is the statistical weight due to nuclear spin of the lower level (1 for *s*-type levels and 3 for *a*-type levels); $\nu_0$ is the transition wavenumber in cm$^{-1}$; $g_V$ depends on the degeneracy of the levels involved, with the convention $g_V$ equals 2 if both upper and lower vibrational states are degenerate and equals 1 otherwise; $Q(T_0)$ is the total partition function at temperature $T_0$, calculated from Fischer et al [24]; $L(J,\ell)$ is the Hönl-London factor; $E''$, in cm$^{-1}$, is the energy of the lower level taken from HITRAN [17]; $k$ is Boltzmann's constant equal to $1.380658 \times 10^{-16}$ erg K$^{-1}$.

Among the 8 studied bands, 4 are parallel ones (3 of them being $\ell$-type doubled) and 4 are forbidden ones. Only one *Q*-branch could be observed. For *P*- and *R*-branches of parallel bands ($\Delta\ell = 0$) and of forbidden ones ($\Delta\ell = \pm 2$), the Hönl-London factor is taken as in Ref. [9]

$$L(J,\ell) = (J+1+\ell)\,(J+1-\ell) \,/\, (J+1) \text{ (for } R\text{-branch)}, \quad (2)$$

$$L(J,\ell) = (J+\ell)\,(J-\ell) \,/\, J \text{ (for } P\text{-branch)}, \quad (3)$$

whereas for the *Q*-branch of the forbidden band with $\Delta\ell = +2$ and $\ell = 0$, it is taken as

$$L(J,\ell) = (2J+1) \,/\, 2. \quad (4)$$

To reduce the data, effective parameters can be deduced expanding $|R|^2$ to take into account the rotational dependence and resonances. For all the bands studied in the present work, the following empirical Herman-Wallis-type factors have been tried

$$|R|^2 = |R_0|^2\,(1 + A_1^{PR}\,m + A_2^{PR}\,m^2)^2\,F' \text{ (for } P\text{- and } R\text{-branches)}, \quad (5)$$

$$|R|^2 = |R_0|^2\,(1 + A_2^{Q}\,m^2)^2\,F' \text{ (for the } Q\text{-branch)}, \quad (6)$$

$m$ being equal to $-J$ in the *P*-branch, $J$+1 in the *R*-branch, and $J$ in the *Q*-branch. $|R_0|^2$ is the vibrational transition dipole moment squared, and $A_1^{PR}$, $A_2^{PR}$, and $A_2^{Q}$, are Herman-Wallis coefficients. Note that the terms between parentheses in Eqs. (5,6) are squared in the present work. Moreover,

$$F' = 1 \text{ for } \Delta\ell = 0. \quad (7)$$

For $\Delta\ell = \pm 2$, $F'$ is taken as

$$F' = [m\,(m+1)]^2. \quad (8)$$

The case of the two strong bands $(\nu_4 + \nu_5)^0_+$ and $(\nu_4 + \nu_5)^2$, for which line intensities were already measured by Vander Auwera [9], desserves a discussion. For $(\nu_4 + \nu_5)^0_+$, line assignments and measurements of positions were performed by Kabbadj et al [2] up to *P*43 and *R*41, and line intensities were measured in Ref. [9] up to *P*35 and *R*35. As we needed relatively large values of the product "pressure × absorbing path length" in order to study weak bands, most of the lines measured by Vander Auwera are saturated in our spectra, so that we could measure only 10 lines that overlap the set of lines studied in Ref. [9] and reported in HITRAN [17]. However, the advantage of spectra with large pressure × absorbing path length product is that we could enlarge the set of intensity data up to *P*43 and *R*45, increasing *J* by about 10 in each branch (see Table 3). Then, we have calculated $|R|^2$ values from the experimental intensities reported in Ref. [9], averaging them when, for a line, several values coming from different spectra had been quoted, and converting them to pure $^{12}C_2H_2$ in cm molecule$^{-1}$ at 296 K. (The obtained values are equal to those given in Ref. [9] ± a few 0.1%, because of roundings and averaging of line intensities, and because of a slight difference between the total partition functions used in Ref. [9] and in the present work. Note that in Table 2 of Ref. [9], the listed $|R|^2$ values are given for natural abundances.) $|R|^2$ values such obtained are plotted on Fig. 1 together with ours. Experimental values deduced from the line intensities of Lepère et al [11] have also been plotted (we have chosen those obtained from a Rautian profile in Ref. [11]). Though the presence of resonances calls for a rigourous theoretical model such these of Refs. [9,25,26], Fig. 1 shows that an effective treatment through an Herman-Wallis factor is powerful and allows to calculate the spectrum with enough precision for most applications (RMS of the fit smaller than 2.7%). To get improved values of $|R_0|^2$ and of Herman-Wallis coefficients, $|R|^2$ values from this work (26 values) and from Ref. [9] (40 values) have been fitted together. The obtained constants are listed in Table 5. A fit merging data from this work and from Refs. [9] and [11] has also been performed. It gave very similar results but degraded slightly the quality of the residuals. Table 5 shows that the retrieved $|R_0|^2$ value is very close to this given in Ref. [9], however keeping in mind the fact that these two values are not strictly comparable since coming from different theoretical models.

As far as the $(\nu_4 + \nu_5)^2$ band is concerned, line intensities could be measured for 83 lines (see Table 4), compared with 24 in Ref. [9]. Particularly, *P*- and *R*-branches are now known from *P*4 to *P*45 and from *R*6 to *R*41. Let us recall that in Ref. [10] a good agreement was found between intensities of 28 lines of $(\nu_4 + \nu_5)^0_+$ measured from Fourier transform spectra recorded at GSMA (Groupe de Spectrométrie Moléculaire et Atmosphérique, Reims) and in Ref. [9], namely −1.5(30)%, with 1 standard deviation (noted 1SD in the following) between parenthesis in unit of the last digit. Such a comparison is not so easy in the present work since the orders of magnitude of line intensities to compare are very different in the two works. For example, intensities of *Q*-lines of $(\nu_4 + \nu_5)^2$, for which large systematic negative discrepancies up to about −40% are observed with Ref. [9] (see Fig. 2), cannot lead to a significant comparison since it involves lines having intensities smaller than about $5 \times 10^{-23}$ cm molecule$^{-1}$, and then weak and difficult to measure in Ref. [9]. If one compares common results between this work and Ref. [9], disregarding Q-lines, i.e., considering only 22 *P*- and *R*-lines of the $(\nu_4 + \nu_5)^0_+$ and $(\nu_4 + \nu_5)^2$

bands, one finds a mean difference of –1.9(30)% between our results and those of Ref. [9]. If one compares the results of Refs. [11] and [9], for 14 common lines, one finds –1.6(30)%, that is very close to the above differences. These are very acceptable agreements, with a small dispersion of the differences (1 SD 3%), if one takes into account the accuracies announced in the concerned works.

One should note that the $R^2$ values of the $(\nu_4 + \nu_5)^2$ forbidden bands cannot be modelled by Eqs. (5,6,8), because of the intensity asymmetry observed between the *P*- and *R*-branches, due to the $\ell$-type resonance and Coriolis coupling already pointed out in Ref. [9]. Values in the *Q*-branch can be smoothed with enough precision for applications by using a polynomial of the second degree, but the coefficients of this polynomial have no physical meaning. Conversely, values in the *P*- and *R*-branches cannot be adjusted by a polynomial, even of high degree, without losing the precision of the experimental data. So, in order to generate a line list for applications, we thought preferable to keep the *P*- and *R*-experimental $|R|^2$ values and to simply smooth, by linear interpolations, the values of missing lines and of a few lines for which $|R|^2$ slightly departs from the general tendency of variation of neighbooring lines. $|R|^2$ values of a few low *J* missing lines have also been obtained by this way. However, no extrapolation of line intensities toward high *J* should be performed for this band.

In Ref. [2], Kabbadj et al assigned 14 lines of the $(2\nu_4 + 2\nu_5)^0_- - (\nu_4 + \nu_5)^2$ forbidden band, i.e., 11 *R*-lines (from *R*13 to *R*23), and 3 *P*-lines (*P*11, *P*12, and *P*13). All *P*-lines fall in very dense bunches of lines, so that we could neither assign new lines nor measure intensities in this branch. Conversely, it has been possible to measure the intensities of 8 *R*-lines already known from Kabbadj et al, plus 3 new *R*-lines (*R*10, *R*11, and *R*12). Experimental $|R|^2$ values have been obtained from the measured intensities using Eqs. (1-3) and could be reduced using Eqs. (5,8). The obtained constants are given in Table 5. These constants should not be considered as true vibrational transition moment squared and Herman-Wallis coeffcients, since our set of experimental data is somewhat poor: intensities could be measured in only one branch, and the set of *J* values is limited and narrow (from 10 to 23). Therefore, the very small value of $|R_0|^2$ has a large absolute uncertainty, at least 20%. However, these constants are efficient to reproduce the data. For that, one needs to take into account 4 digits in these constants because of terms of high degree of *m* in Eqs. (5,8). Consequently, no extrapolation of line intensities toward high *J* should be performed. All results concerning this band are given tentatively.

The $(2\nu_4 + 2\nu_5)^2$ II $- (\nu_4 + \nu_5)^0_-$ forbidden band was known by 28 lines assigned by Kabbadj et al [2], i.e., *P*13 to *P*25 and *R*11 to *R*26. We could measure line intensities for 43 lines in a more extended set of *J* values, from *P*5 to *P*33 and from *R*3 to *R*32. Experimental $|R|^2$ values have been obtained using Eqs. (1-3) but could not be fitted by Eqs. (5,8). However, as shown on Fig. 3, the precision of these values is good enough to allow to smooth them as performed for the $(\nu_4 + \nu_5)^2$ band.

The last forbidden band is $(2\nu_4 + \nu_5)^3 - \nu_4{}^1$, that is of the $\Phi \leftarrow \Pi$ type, and for which only *f*-levels are involved. Kabbadj et al [2] assigned 28 lines in this band, from *P*16 to *P*29, and from *R*12 to *R*28. We have been able to measure line intensities in a slightly more extended domain of *J* values, namely from *P*10 to *P*32, and from *R*12 to *R*28. Furthermore, the positions of some lines could be noticeably improved, e.g., *R*13, *R*16, or *R*17. However, numerous lines of this band are hidden by stronger ones of other bands. This is unfortunately the case for several lines of low *J* values (*J* smaller than 10). As for other forbidden bands, the experimental $|R|^2$ values could not be fitted by Eqs. (5,8), so that we needed to smooth the values by linear

interpolations. As overlappings and blends are particularly numerous for the lines of this band, we had to remove those of them for which some difficulty in the measurement process would had as consequence to lead to too dispersed $|R|^2$ values. Then, interpolations were easier.

The $(2\nu_4 + \nu_5)^1$ II – $\nu_4{}^1$ band is one of the strongest bands after $(\nu_4 + \nu_5)^0{}_+$ and $(\nu_4 + \nu_5)^2$. Its strongest lines (having $J$ between about 4 and 18) are saturated in all our spectra and therefore could not be measured. However, a few lines with low $J$ values ($J$ = 1, 2, or 3) could be measured. Added to numerous lines having $J$ greater than about 19 and up to *Pe*37 and *Rf*42 (see Table 3), they allow a significant determination of a vibrational transition dipole moment squared and Herman-Wallis coefficients. Indeed, the transition dipole moment squared has no important rotational dependence for this band (see Fig. 4), so that the lack of data in the middle of *P*- and *R*-branches is not a drawback. The two *e* and *f* sub-bands have been fitted simultaneously, giving rise to a common value for the vibrational transition dipole moment squared but to distinct Herman-Wallis coefficients (see Table 5). Note that $A_2{}^{PR}$ of the *e* sub-band could not be determined significantly and was fixed at zero. Such a data reduction is typical of the other bands with $\ell$-type doubling. Figure 5 is an interesting example showing the strong and opposite rotational dependences of the sub-bands of $(2\nu_4 + \nu_5)^1$ I – $\nu_4{}^1$.

The remaining bands presented in this paper have been studied in the same manner. The spectra being very crowded, one should note that numerous lines could not be measured, e.g., because of unresolved overlappings, but that it was not a drawback to account for the rotational dependence of $|R|^2$ (see Figs. 4,5) for most of the bands. The complete list of line intensities is given in the supplementary material.

## 4. Line list for applications

The obtained results show that a global model, taking into account the numerous resonances, will be necessary to generate a precise synthetic spectrum, especially to account for the case of the forbidden bands. However, such a model cannot operate so long as line intensities of the other remaining weak bands are not measured. That is why, to benefit from the results of the present work, we choose to set up a line list in the HITRAN format that could be used even now for applications. Presently, HITRAN only contains data for the $(\nu_4 + \nu_5)^0{}_+$ band from Ref. [9].

The line list has been established in the same way as in Refs. [27,28]. As the present work was not specifically dedicated to line position measurements, we have relied on the best values existing in the literature. For the $(\nu_4 + \nu_5)^0{}_+$ band, we have picked up the line positions calculated by Vander Auwera [9] using the constants of Ref. [2], as they are given in HITRAN [17] from *P*35 to *R*35. For the other bands, the experimental line positions of Kabbadj et al [2] have been retained. For lines not observed in Refs. [2,9], as for a few lines that could be treated in a better way in our spectra, the positions obtained by the multispectrum procedure have been taken. For the missing lines and for a few extrapolated ones, positions have been obtained using an effective model based on a polynomial adjustment of the experimental line positions of Refs. [2,9] together with additional lines of this work if any.

To generate line intensities, vibrational transition dipole moments squared and Herman-Wallis coefficients (see Table 5) have been used to calculate $|R|^2$ values and then the intensities. Table 3 and the supplementary material show that the residuals are smaller than 3% on the average, and therefore are acceptable for usual applications. Line intensities corresponding to a

few higher values of $J$ (about 5 additional values) have been extrapolated for some bands, their uncertainty codes being degraded consequently. To calculate the intensities of these additional lines, $|R|^2$ has been fixed at the value calculated for the highest observed $J$ line in each band. As far as the $(\nu_4 + \nu_5)^0_+$ band is concerned, intensities calculated by Vander Auwera [9] from his absolute measurements, through a rigorous treatment, have been picked up. Line intensities of additional lines measured in this work for this band have been calculated using the constants of Table 5. Note that the statistical weights and the Einstein-$A$ coefficients already present in HITRAN have also been picked up for these lines (Einstein-$A$ coefficients have been put in place of $|R|^2$ values in this case). For the $(\nu_4 + \nu_5)^2$ forbidden band, smoothed values of $|R|^2$ have been used to calculate line intensities. These smoothed values can be found in the line list. No extrapolation toward high $J$ has been performed for this band. For the $(2\nu_4 + 2\nu_5)^0_- - (\nu_4 + \nu_5)^2$ forbidden band, the constants of Table 5 have been used, without extrapolation toward high $J$. Low $J$ missing lines have been calculated in the $R$-branch, as well as $P$-lines from $P2$ to the last line, $P13$, observed in Ref. [2]. Calculated intensities of these lines have an absolute uncertainty of at least 20% and are given tentatively in the line list. For the $(2\nu_4 + \nu_5)^3 - \nu_4{}^1$ forbidden band, we have proceeded similarly. However, because of the lack of measurements between $P10$ and $R12$, the extrapolation of $|R|^2$ is difficult for the missing low $J$ lines. As is usually done when one wants to extrapolate the intensities of weak high $J$ lines, we chose not to take into account the rotational dependence of $|R|^2$ between $P10$ and $R12$: in the $P$-branch and for $J$ smaller than 10, $|R|^2$ is fixed at the value measured for $P10$, whereas in the $R$-branch and for $J$ smaller than 13, $|R|^2$ is fixed at the value measured for $R13$. This has no great consequence for applications since the concerned lines are weak, but the uncertainty of their intensity given in the line list has been increased (possibly more than 20%).

Other spectroscopic data are the same as those already put in the last updates of the databases: air- and self-broadening coefficients, default value for the temperature exponent of air-broadening coefficients, constant value for the air-pressure shifting coefficient, and their accuracies [17,29]. Table 6 summarizes the data now available for the $^{12}C_2H_2$ molecule in the studied spectral region. To facilitate comparisons, this table has been set up in the same format as in Refs. [27,28]. This line list contains 784 transitions and is included in the supplementary material.

## 5. Conclusion

Absolute intensities have been measured for more than 400 lines in 8 bands of the $^{12}C_2H_2$ spectrum around 7.7 µm, including the strongest bands. For allowed bands, an effective model of Herman-Wallis factor has been applied to model the spectrum with a satisfactory precision (better than 5% on the mean). For some forbidden bands, experimental values had to be smoothed by linear interpolations. A line list containing 784 transitions has been set up in the HITRAN format, which can be helpful for applications even now. However, an important work has still to be performed to study line intensities in some ten weaker hot bands observable in the recorded spectra. Once acquired, such a set of line intensities can be treated by a global model, as this of Perevalov et al (see, e.g., Refs. [25,26]), able to take into account the numerous resonances between levels involved in the 7.7 µm spectral region and to account for the forbidden bands.

**References**


[1] El Idrissi MI, Liévin J, Campargue A, Herman M. The vibrational energy pattern in acetylene (IV): updated global vibration constants for $^{12}C_2H_2$. J Chem Phys 1999;110:2074-86.

[2] Kabbadj Y, Herman M, Di Lonardo G, Fusina L, Johns JWC. The bending energy levels of $C_2H_2$. J Mol Spectrosc 1991;150:535-65.

[3] Robert S, Herman M, Vander Auwera J, Di Lonardo G, Fusina L, Blanquet G, Lepere M, Fayt A. The bending vibrations in $^{12}C_2H_2$: global vibration-rotation analysis. Mol Phys 2007;105:559-68. Robert S, Herman M, Vander Auwera J, Di Lonardo G, Fusina L, Blanquet G, Lepere M, Fayt A. Erratum. Mol Phys 2007;105:2009.

[4] Kelly R, Rollefson R, Schurin BS. The infrared dispersion of acetylene and the dipole moment of the C-H bond. J Chem Phys 1951;19:1595-9.

[5] Varanasi P, Bangaru BRP. Measurement of integrated intensities of acetylene bands in the 3.04, 7.53, and 13.7 µm. JQSRT 1974;14:839-44.

[6] Koops T, Smit WMA, Visser T. Measurement and interpretation of the absolute infrared intensities of acetylene: fundamentals and combination bands. J Mol Struct 1984;112:285-99.

[7] Abbouti Temsamani M, Champion JM, Oss S. Infrared transition intensities in acetylene : an algebraic approach. J Chem Phys 1999;110:2893-902.

[8] Podolske JR, Lœwenstein M, Varanasi P. Diode laser line strength measurements of the $(\nu_4 + \nu_5)^0$ band of $^{12}C_2H_2$. J Mol Spectrosc 1984;107:241-9.

[9] Vander Auwera J. Absolute intensities measurements in the $(\nu_4 + \nu_5)$ band of $^{12}C_2H_2$: analysis of Herman-Wallis effects and forbidden transitions. J Mol Spectrosc 2000;201:143-50.

[10] Jacquemart D, Mandin JY, Dana V, Régalia-Jarlot L, Thomas X, Von der Heyden P. Multispectrum fitting measurements of line parameters for 5-µm cold bands of acetylene. JQSRT 2002;75:397-422.

[11] Lepère M, Blanquet G, Walrand J, Bouanich JP, Herman M, Vander Auwera J. Self-broadening coefficients and absolute line intensities in the $\nu_4 + \nu_5$ band of acetylene. J Mol Spectrosc 2007;242:25-30.

[12] Varanasi P, Giver LP, Valero FPJ. Measurements of nitrogen-broadened line widths of acetylene at low temperatures. JQSRT 1983;30:505-9.

[13] Devi VM, Benner DC, Rinsland CP, Smith MAH, Sidney BD. Tunable diode laser measurements of N2- and air-broadened half-widths: lines in the $(\nu_4 + \nu_5)^0$ band of $^{12}C_2H_2$ near 7.4 µm. J Mol Spectrosc 1985;114:49-53.

[14] Fissiaux L, Dhyne M, Lepère M. Diode-laser spectroscopy : Pressure dependence of $N_2$-broadening coefficients of lines in the $\nu_4 + \nu_5$ band of $C_2H_2$. J Mol Spectrosc 2009;254:10-5.

[15] Dhyne M, Fissiaux L, Populaire JC, Lepère M. Temperature dependence of the $N_2$-broadening coefficients of acetylene. JQSRT 2009;110:358-66.

[16] Matsuura M, Wood PR, Sloan GC, Zijlstra AA. Spitzer observations of acetylene bands in carbon-rich asymptotic giant branch stars in the Large Magellanic Cloud. Mon Not R Astron Soc 2006;371:415-20.

[17] Rothman LS, Gordon IE, Barbe A, Chris Benner D, et al. The HITRAN 2008 Molecular Spectroscopic database. JQSRT 2009;110,533-572.

[18] Jacquinet-Husson N, Scott NA, Chédin A, Garceran K, et al. The 2003 edition of GEISA / IASI spectroscopic database. JQSRT 2005;95:429-67.

[19] Wartewig S. IR and Raman Spectroscopy: Fundamental Processing. Weinheim: Wiley-VCH; 2003.

[20] Mertz L. Transformations in Optics. New York: Wiley; 1965.

[21] Griffiths PR, deHaseth JA. Fourier Transform Infrared Spectrometry. New York: Wiley; 1986.

[22] Jacquemart D, Mandin JY, Dana V, Picqué N, Guelachvili G. A multispectrum fitting procedure to deduce molecular line parameters. Application to the 3–0 band of $^{12}C^{16}O$. Eur Phys J D 2001;14:55-69.

[23] Jacquemart D, Mandin JY, Dana V, Régalia-Jarlot L, Plateaux JJ, Décatoire D, Rothman LS. The spectrum of acetylene in the 5-µm region from new line-parameter measurements. JQSRT 2003;76:237-67.

[24] Fischer J, Gamache RR, Goldman A, Rothman LS, Perrin A. Total internal partition sums for molecular species in the 2000 edition of the HITRAN database. JQSRT 2003;82:401-12.

[25] Perevalov VI, Lobodenko EI, Teffo JL. Reduced effective Hamiltonian for global fitting of $C_2H_2$ rovibrational lines. In: Proceedings of the XIIth Symposium and School on High-Resolution Molecular Spectroscopy, St. Petersburg. SPIE 1997;3090:143-9.

[26] Perevalov VI, Lyulin OM, Jacquemart D, Claveau C, Teffo JL, Dana V, et al. Global fitting of line intensities of acetylene molecule in the infrared using the effective operator approach. J Mol Spectrosc 2003;218:180–9.

[27] Jacquemart D, Lacome N, Mandin JY, Dana V, Tran H, Gueye FK, Lyulin OM, Perevalov VI, Régalia-Jarlot L. The IR spectrum of $^{12}C_2H_2$: line intensity measurements in the 1.4 µm region and update of the databases. JQSRT 2009;110:717–732.

[28] Jacquemart D, Lacome N, Mandin JY. Line intensities of $^{12}C_2H_2$ in the 1.3, 1.2, and 1 µm spectral regions. JQSRT 2009;110,733-742.

[29] Jacquemart D, Lacome N, Mandin JY, Dana V, Lyulin OM, Perevalov VI. Multispectrum fitting procedure for $^{12}C_2H_2$ in the 3.8-µm spectral region. JQSRT 2007;103:478-95.

**Captions of Tables**

Table 1
List of the bands observed by Kabbadj et al [2] in the $\Delta P = 2$ series of transitions of $^{12}C_2H_2$ around 7.7 μm

Table 2
Experimental conditions and characteristics of the spectra recorded around 7.7 μm using the rapid-scan interferometer in Paris (LADIR)

Table 3
Line positions and intensities for selected allowed bands of the $^{12}C_2H_2$ molecule in the 7.7 μm region.

Table 4
Line positions and intensities for the forbidden $(\nu_4 + \nu_5)^2$ band of the $^{12}C_2H_2$ molecule in the 7.7 μm region.

Table 5
Summary of $^{12}C_2H_2$ experimental vibrational transition dipole moments squared $|R_0|^2$ in $D^2$ ($1\ D = 3.33546 \times 10^{-30}$ C m), and Herman-Wallis coefficients, see Eqs. (2-8), in the 7.7 μm spectral region

Table 6
Summary of new bands and transitions available for the $^{12}C_2H_2$ molecule at 7.7 μm

**Captions of Figures**

Fig. 1. Variation of the transition dipole moment squared $|R|^2$, in $D^2$ ($1\ D = 3.33546 \times 10^{-30}$ C m), vs. *m*, for the $(\nu_4 + \nu_5)^0_+$ band. Solid triangles are experimental values obtained in this work. Solid squares are experimental values deduced from intensities measured by Vander Auwera [9] (when several values, coming from different spectra, are given for a line in Ref. [9], they have been averaged). Open triangles are experimental values deduced from intensities measured by Lepère et al [11]. (Experimental intensities quoted in Refs. [9,11] were preliminarily converted for a sample of 100% of $^{12}C_2H_2$.) The solid line represents the values calculated using the constants reported in Table 5. They result from an unweighted fit including the experimental data of this work and those of Vander Auwera [9] (see Section 3).

Fig. 2. Variation of the transition dipole moment squared $|R|^2$, in $D^2$ ($1\ D = 3.33546 \times 10^{-30}$ C m), vs. *m*, for the $(\nu_4 + \nu_5)^2$ band. Solid triangles are experimental values obtained in this work. Open triangles are experimental values deduced from intensities measured by Vander Auwera [9]. The upper plot shows *P*-and *R*-branches whereas the lower plot shows the *Q*-branch.

Fig. 3. Variation of the transition dipole moment squared $|R|^2$, in $D^2$ ($1\ D = 3.33546 \times 10^{-30}$ C m), vs. *m*, for the $(2\nu_4 + 2\nu_5)^2$ II – $(\nu_4 + \nu_5)^0_-$ band. Solid triangles are experimental values obtained in this work.

Fig. 4. Variation of the transition dipole moment squared $|R|^2$, in $D^2$ ($1\ D = 3.33546 \times 10^{-30}$ C m), vs. *m*, for the $(2\nu_4 + \nu_5)^1$ II – $\nu_4{}^1$ band. Solid triangles are experimental values obtained in the *e* sub-band, and open ones in the *f* sub-band. The lines represent the values calculated using the constants reported in Table 5. The solid line is for the *e* sub-band, and the dashed one for the *f* sub-band.

Fig. 5. Variation of the transition dipole moment squared $|R|^2$, vs. *m*, for the $(2\nu_4 + \nu_5)^1$ I – $\nu_4{}^1$ band. See caption of Fig. 4.

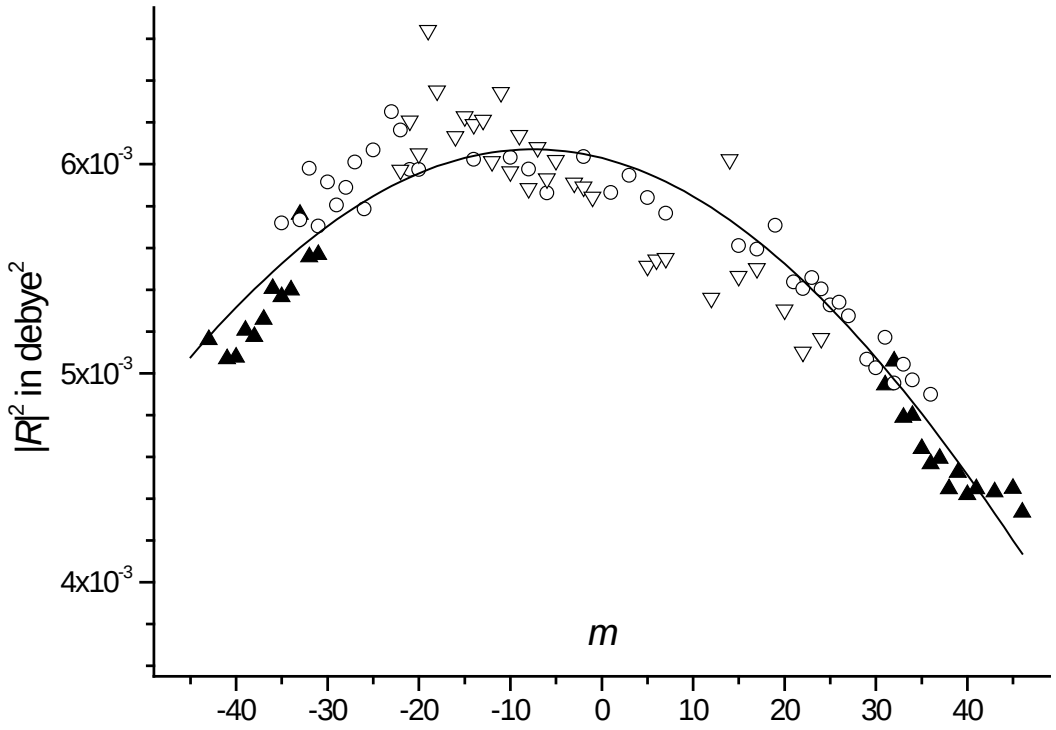


Fig. 1. Variation of the transition dipole moment squared $|R|^2$, in $D^2$ (1 D = 3.33546 × $10^{-30}$ C m), vs. *m*, for the $(\nu_4 + \nu_5)^0_+$ band. Solid triangles are experimental values obtained in this work. Open circles are experimental values deduced from intensities measured by Vander Auwera [9] (when several values, coming from different spectra, are given for a line in Ref. [9], they have been averaged). Open triangles are experimental values deduced from intensities measured by Lepère et al [11]. (Experimental intensities quoted in Refs. [9,11] were preliminarily converted for a sample of 100% of $^{12}C_2H_2$.) The solid line represents the values calculated using the constants reported in Table 5. They result from an unweighted fit including the experimental data of this work and those of Vander Auwera [9] (see Section 3).

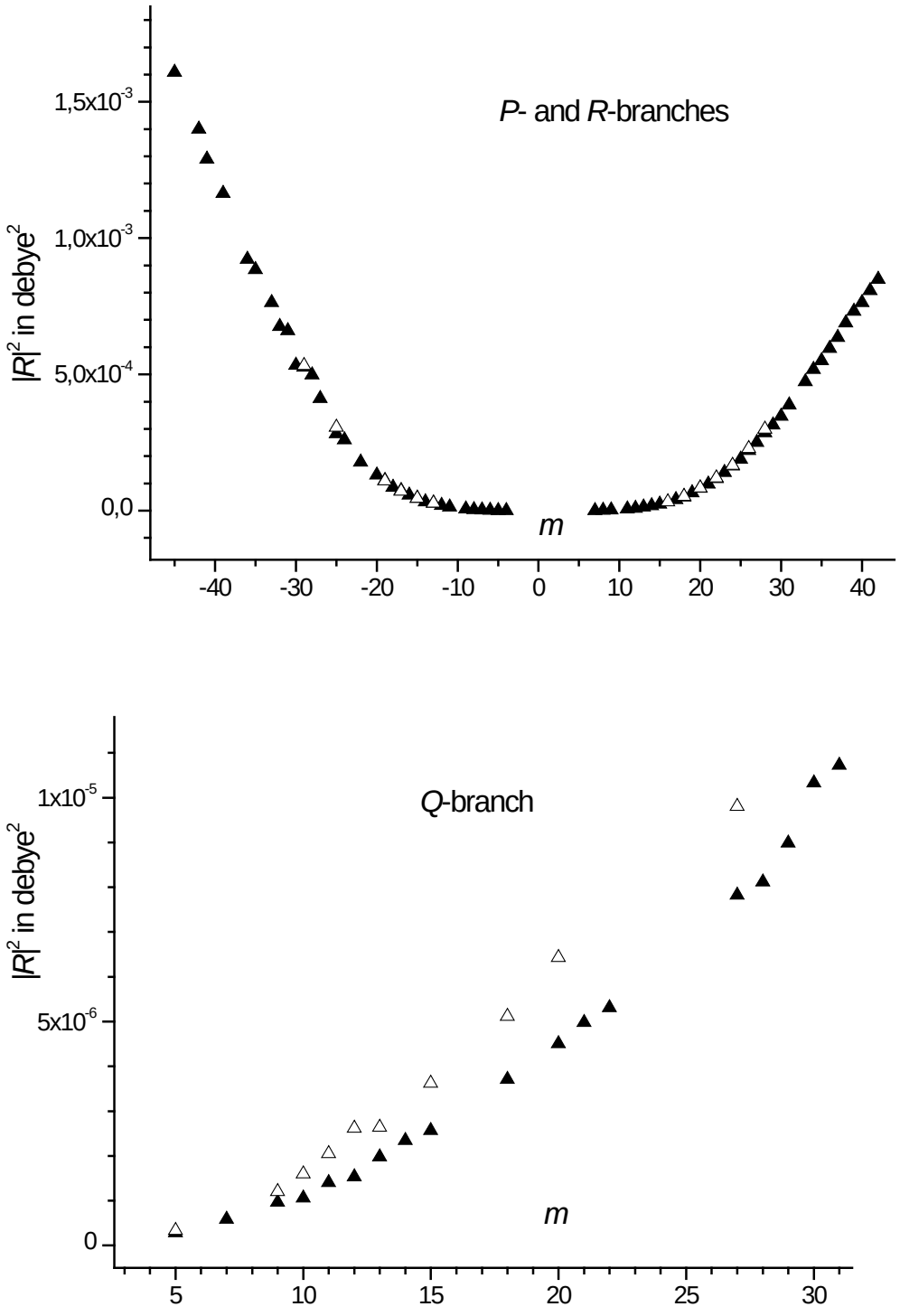


Fig. 2. Variation of the transition dipole moment squared $|R|^2$, in $D^2$ (1 D = 3.33546 × $10^{-30}$ C m), vs. *m*, for the $(\nu_4 + \nu_5)^2$ band. Solid triangles are experimental values obtained in this work. Open triangles are experimental values deduced from intensities measured by Vander Auwera [9]. The upper plot shows *P*-and *R*-branches whereas the lower plot shows the *Q*-branch.

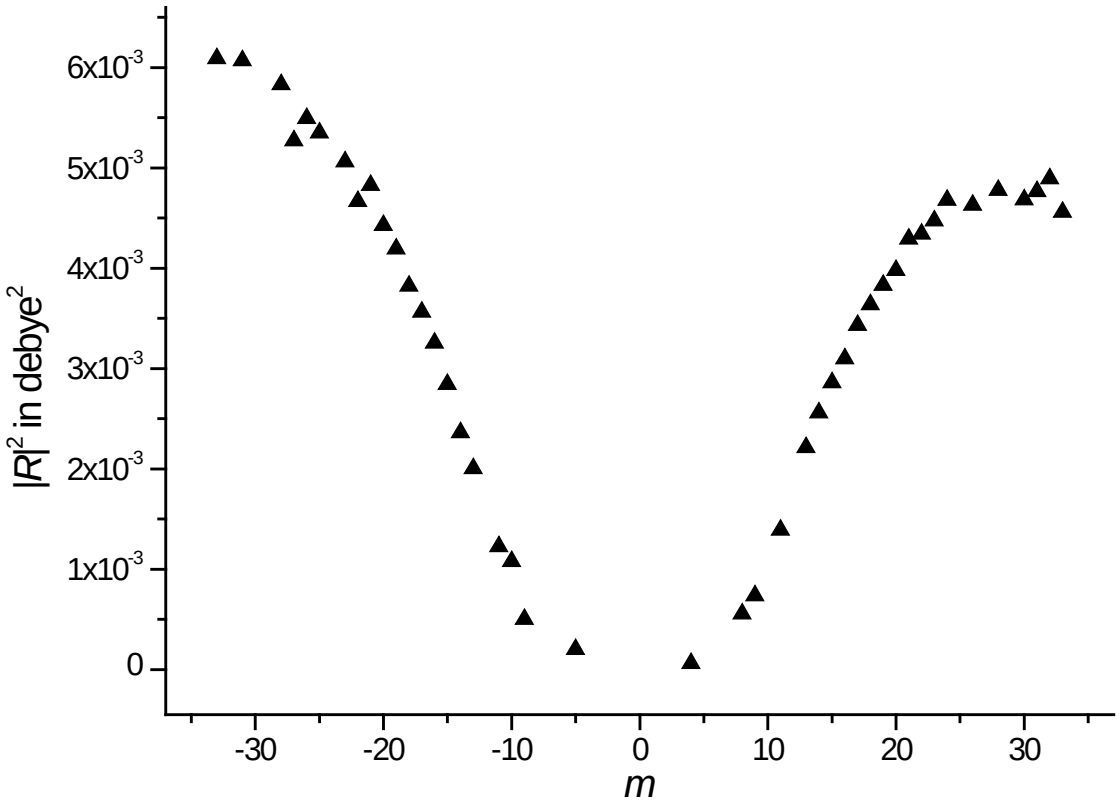


Fig. 3. Variation of the transition dipole moment squared $|R|^2$, in $D^2$ (1 D = 3.33546 × $10^{-30}$ C m), vs. *m*, for the $(2\nu_4 + 2\nu_5)^2$ II – $(\nu_4 + \nu_5)^0$ band. Solid triangles are experimental values obtained in this work.

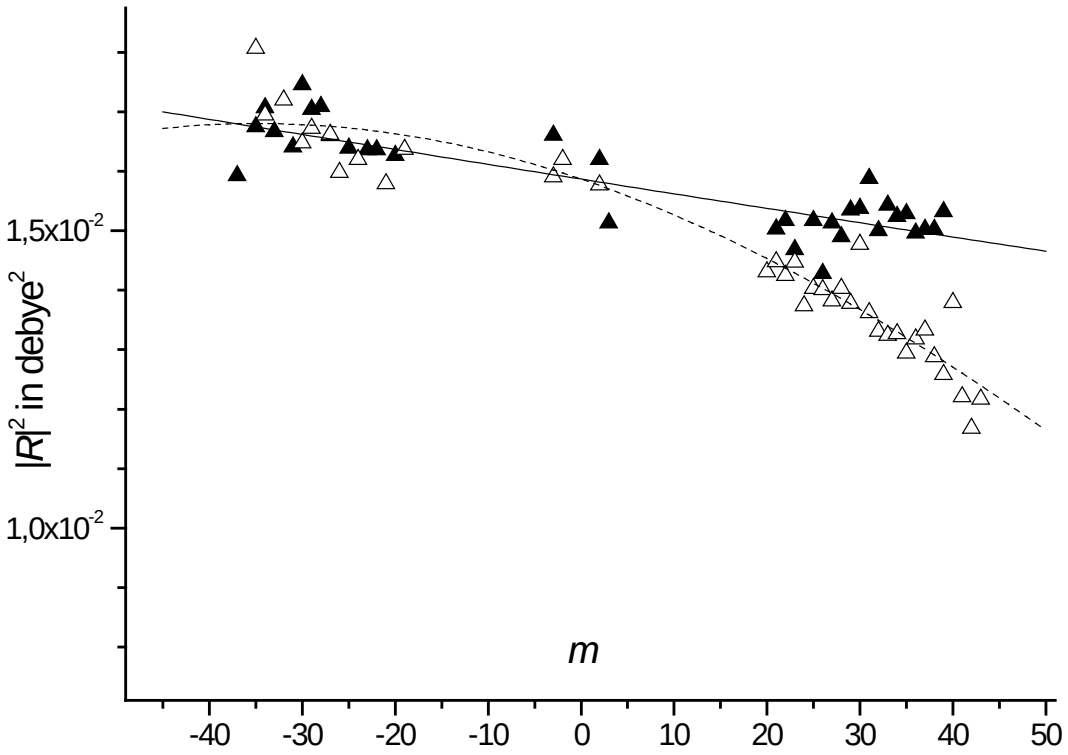


Fig. 4. Variation of the transition dipole moment squared $|R|^2$, in $D^2$ (1 D = 3.33546 × $10^{-30}$ C m), vs. *m*, for the $(2\nu_4 + \nu_5)^1\,\Pi - \nu_4{}^1$ band. Solid triangles are experimental values obtained in the *e* sub-band, and open ones in the *f* sub-band. The lines represent the values calculated using the constants reported in Table 5. The solid line is for the *e* sub-band, and the dashed one for the *f* sub-band.

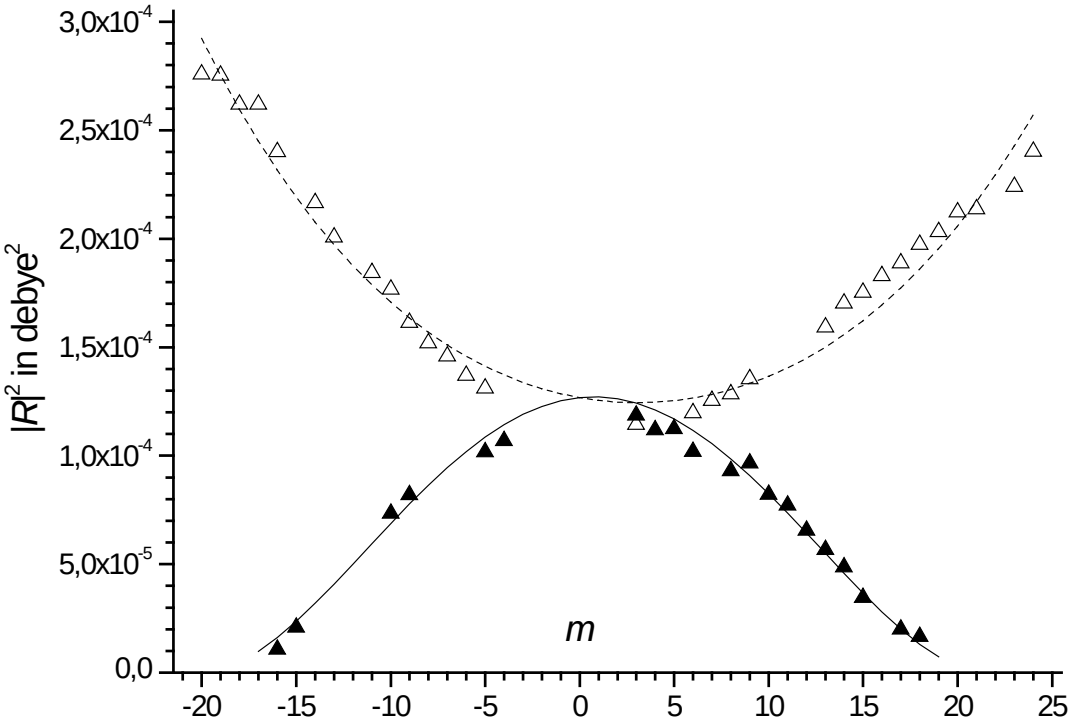


Fig. 5. Variation of the transition dipole moment squared $|R|^2$, vs. $m$, for the $(2\nu_4 + \nu_5)^1$ I – $\nu_4{}^1$ band. See caption of Fig. 4.

Table 1

List of the bands observed by Kabbadj et al [2] in the $\Delta P = 2$ series of transitions of $^{12}C_2H_2$ around 7.7 μm

| Band | Center [a] | Upper level [b] | Polyad [b] | Symmetry |
|---|---|---|---|---|
| $\nu_2 - \nu_5^1$ | 1245.140 | $010(00)^0_+$ | $\{3\nu_5\}$ | $\Sigma^+_g \leftarrow \Pi_u$ |
| $(\nu_4 + 3\nu_5)^0_+ - 2\nu_5^0$ | 1308.686 | $000(13)^0_+$ | $\{4\nu_5\}$ | $\Sigma^+_u \leftarrow \Sigma^+_g$ |
| $(\nu_4 + 3\nu_5)^2 - 2\nu_5^2$ | 1310.182 | $000(13)^2$ | $\{4\nu_5\}$ | $\Delta_u \leftarrow \Delta_g$ |
| $(2\nu_4 + 2\nu_5)^0_- - (\nu_4 + \nu_5)^2$ | 1311.308 | $000(22)^0_- f$ | $\{4\nu_5\}$ | $\Sigma^-_g \leftarrow \Delta_u$ |
| $(2\nu_4 + 2\nu_5)^2$ II $- (\nu_4 + \nu_5)^2$ | 1318.652 | $000(22)^2$ II | $\{4\nu_5\}$ | $\Delta_g \leftarrow \Delta_u$ |
| $(\nu_4 + 2\nu_5)^1$ II $- \nu_5^1$ | 1318.730 | $000(12)^1$ II | $\{3\nu_5\}$ | $\Pi_g \leftarrow \Pi_u$ |
| $(2\nu_4 + 2\nu_5)^0_+ - (\nu_4 + \nu_5)^0_+$ | 1319.942 | $000(22)^0_+$ | $\{4\nu_5\}$ | $\Sigma^+_g \leftarrow \Sigma^+_u$ |
| $(2\nu_4 + 2\nu_5)^0_- - (\nu_4 + \nu_5)^0_-$ | 1320.638 | $000(22)^0_-$ | $\{4\nu_5\}$ | $\Sigma^-_g \leftarrow \Sigma^-_u$ |
| $(2\nu_4 + 2\nu_5)^2$ II $- (\nu_4 + \nu_5)^0_-$ | 1320.908 | $000(22)^2$ II $f$ | $\{4\nu_5\}$ | $\Delta_g \leftarrow \Sigma^-_u$ |
| $(3\nu_4 + \nu_5)^2 - 2\nu_4^2$ | 1328.019 | $000(31)^2$ | $\{4\nu_5\}$ | $\Delta_u \leftarrow \Delta_g$ |
| $(\nu_4 + \nu_5)^0_+$ | 1328.081 | $000(11)^0_+$ | $\{2\nu_5\}$ | $\Sigma^+_u \leftarrow \Sigma^+_g$ |
| $(2\nu_4 + \nu_5)^1$ II $- \nu_4^1$ | 1328.314 | $000(21)^1$ II | $\{3\nu_5\}$ | $\Pi_u \leftarrow \Pi_g$ |
| $(3\nu_4 + \nu_5)^0_+ - 2\nu_4^0$ | 1330.206 | $000(31)^0_+$ | $\{4\nu_5\}$ | $\Sigma^+_u \leftarrow \Sigma^+_g$ |
| $(\nu_4 + 2\nu_5)^1$ I $- \nu_5^1$ | 1336.644 | $000(12)^1$ I | $\{3\nu_5\}$ | $\Pi_g \leftarrow \Pi_u$ |
| $(\nu_4 + \nu_5)^2$ | 1342.821 | $000(11)^2 e$ | $\{2\nu_5\}$ | $\Delta_u \leftarrow \Sigma^+_g$ |
| $(2\nu_4 + \nu_5)^1$ I $- \nu_4^1$ | 1348.006 | $000(21)^1$ I | $\{3\nu_5\}$ | $\Pi_u \leftarrow \Pi_g$ |
| $(2\nu_4 + \nu_5)^3 - \nu_4^1$ | 1350.273 | $000(21)^3 f$ | $\{3\nu_5\}$ | $\Phi_u \leftarrow \Pi_g$ |

[a] Band centers, in $cm^{-1}$, have been compiled from Ref. [2].

[b] For each band, the upper vibrational level and the polyad to which it belongs have been quoted. For the 4 forbidden bands, the sub-level (*e* or *f*) observed in Ref. [2] is mentioned. Levels are noted as explained in Section 1.

Table 2

Experimental conditions and characteristics of the spectra recorded around 7.7 μm using the rapid-scan interferometer in Paris (LADIR)

| | |
|---|---|
| Commercial sample (Air Liquide Alphagaz) | |
| Natural $C_2H_2$ | 97.760 % of $^{12}C_2H_2$ |
| Stated purity | 99.55 % |
| Maximum path difference | 180 cm |
| Unapodized FWHM resolution | $\approx 2.8 \times 10^{-3}$ cm$^{-1}$ |
| Spectral step after post-zero filling | $6.3 \times 10^{-4}$ cm$^{-1}$ |
| Number of coadded scans | 400 |
| SNR in the involved spectral domain | ≈ 350 |
| Collimator focal length | 418 mm |
| Nominal iris radius | 0.85 mm |
| Adjusted effective iris radius | 1.00(4) mm [a] |

| Spectrum number | Total pressure (hPa) ±0.5% [b] | Absorbing path (cm) ±1 cm [b] | Temperature (K) ±0.5 K [b] |
|---|---|---|---|
| 1 | 7.585 | 2015 | 297.15 |
| 2 | 2.283 | 2015 | 296.45 |
| 3 | 1.254 | 2015 | 297.15 |
| 4 | 0.8185 | 2015 | 297.85 |
| 5 | 0.4283 | 2015 | 298.35 |
| 6 | 0.1971 | 2015 | 298.95 |

[a] 1 SD between parentheses in unit of the last quoted digit.
[b] Absolute uncertainty (excess digits are given as a guide).

Table 3

Line positions and intensities for selected allowed bands of the $^{12}C_2H_2$ molecule in the 7.7 μm region. [a]

| Line | Position | $S_{obs}$ | $S_{calc}$ | % | $\|R\|^2_{obs}$ |
|---|---|---|---|---|---|
| $(\nu_4 + \nu_5)^0{}_+$ | | | | | |
| Pee43 | 1229.63445 | 1.687E-23 | 1.692E-23 | -0.30 | 5.161E-03 |
| Pee41 | 1234.33025 | 4.174E-23 | 4.339E-23 | -3.95 | 5.069E-03 |
| Pee40 | 1236.66863 | 2.172E-23 | 2.274E-23 | -4.70 | 5.076E-03 |
| Pee39 | 1239.00039 | 1.029E-22 | 1.060E-22 | -3.01 | 5.205E-03 |
| Pee38 | 1241.32569 | 5.194E-23 | 5.422E-23 | -4.39 | 5.176E-03 |
| Pee37 | 1243.64441 | 2.380E-22 | 2.465E-22 | -3.57 | 5.258E-03 |
| Pee36 | 1245.95659 | 1.212E-22 | 1.230E-22 | -1.49 | 5.405E-03 |
| Pee35 | 1248.26226 | 5.300E-22 | 5.457E-22 | -2.96 | 5.366E-03 |
| Pee34 | 1250.56156 | 2.578E-22 | 2.657E-22 | -3.06 | 5.398E-03 |
| Pee33 | 1252.85460 | 1.183E-21 | 1.150E-21 | 2.79 | 5.760E-03 |
| Pee32 | 1255.14166 | 5.382E-22 | 5.458E-22 | -1.41 | 5.557E-03 |
| Pee31 | 1257.42288 | 2.262E-21 | 2.304E-21 | -1.86 | 5.567E-03 |
| Ree30 | 1402.99255 | 1.065E-21 | 1.082E-21 | -1.60 | 4.944E-03 |
| Ree31 | 1405.37220 | 2.373E-21 | 2.332E-21 | 1.73 | 5.058E-03 |
| Ree32 | 1407.74330 | 5.370E-22 | 5.515E-22 | -2.70 | 4.788E-03 |
| Ree33 | 1410.10556 | 1.143E-21 | 1.159E-21 | -1.40 | 4.797E-03 |
| Ree34 | 1412.45877 | 2.579E-22 | 2.672E-22 | -3.61 | 4.639E-03 |
| Ree35 | 1414.80270 | 5.265E-22 | 5.476E-22 | -4.01 | 4.567E-03 |
| Ree36 | 1417.13728 | 1.205E-22 | 1.231E-22 | -2.16 | 4.592E-03 |
| Ree37 | 1419.46238 | 2.363E-22 | 2.463E-22 | -4.23 | 4.447E-03 |
| Ree38 | 1421.77794 | 5.346E-23 | 5.404E-23 | -1.08 | 4.526E-03 |
| Ree39 | 1424.08394 | 1.031E-22 | 1.054E-22 | -2.23 | 4.418E-03 |
| Ree40 | 1426.38037 | 2.252E-23 | 2.256E-23 | -0.18 | 4.446E-03 |
| Ree42 | 1430.94472 | 9.184E-24 | 8.970E-24 | 2.33 | 4.432E-03 |
| Ree44 | 1435.47138 | 3.595E-24 | 3.395E-24 | 5.56 | 4.448E-03 |
| Ree45 | 1437.72060 | 6.449E-24 | 6.154E-24 | 4.57 | 4.334E-03 |
| $(2\nu_4 + \nu_5)^1$ II – $\nu_4{}^1$ | | | | | |
| Pee37 | 1243.41767 | 1.859E-23 | 1.961E-23 | -5.49 | 1.593E-02 |
| Pee35 | 1248.01886 | 4.260E-23 | 4.260E-23 | 0.00 | 1.675E-02 |
| Pee34 | 1250.31348 | 2.099E-23 | 2.056E-23 | 2.05 | 1.707E-02 |
| Pee33 | 1252.60446 | 8.802E-23 | 8.816E-23 | -0.16 | 1.667E-02 |
| Pee31 | 1257.17618 | 1.713E-22 | 1.738E-22 | -1.46 | 1.641E-02 |
| Pee30 | 1259.45762 | 8.384E-23 | 7.982E-23 | 4.79 | 1.746E-02 |
| Pee29 | 1261.73641 | 3.347E-22 | 3.260E-22 | 2.60 | 1.704E-02 |
| Pee28 | 1264.01299 | 1.506E-22 | 1.460E-22 | 3.05 | 1.709E-02 |
| Pee27 | 1266.28762 | 5.836E-22 | 5.817E-22 | 0.33 | 1.660E-02 |
| Pee25 | 1270.83268 | 9.797E-22 | 9.860E-22 | -0.64 | 1.639E-02 |
| Pee23 | 1275.37468 | 1.579E-21 | 1.587E-21 | -0.51 | 1.636E-02 |
| Pee22 | 1277.64554 | 6.551E-22 | 6.575E-22 | -0.37 | 1.636E-02 |
| Pee20 | 1282.18879 | 9.706E-22 | 9.765E-22 | -0.61 | 1.627E-02 |
| Pee 3 | 1321.27042 | 4.209E-21 | 4.040E-21 | 4.02 | 1.661E-02 |
| Ree 1 | 1333.02342 | 2.466E-21 | 2.408E-21 | 2.35 | 1.620E-02 |
| Ree 2 | 1335.38979 | 1.337E-21 | 1.396E-21 | -4.41 | 1.513E-02 |

Table 3 (continued)

| Line | Position | $S_{obs}$ | $S_{calc}$ | % | $\|R\|^2_{obs}$ |
|---|---|---|---|---|---|
| Ree20 | 1378.59278 | 1.013E-21 | 1.035E-21 | -2.17 | 1.503E-02 |
| Ree21 | 1381.00425 | 2.535E-21 | 2.562E-21 | -1.07 | 1.517E-02 |
| Ree22 | 1383.41398 | 6.664E-22 | 6.948E-22 | -4.26 | 1.468E-02 |
| Ree24 | 1388.22619 | 4.395E-22 | 4.420E-22 | -0.57 | 1.517E-02 |
| Ree25 | 1390.62765 | 9.722E-22 | 1.037E-21 | -6.67 | 1.428E-02 |
| Ree26 | 1393.02574 | 2.655E-22 | 2.669E-22 | -0.53 | 1.513E-02 |
| Ree27 | 1395.41954 | 5.992E-22 | 6.106E-22 | -1.90 | 1.490E-02 |
| Ree28 | 1397.80900 | 1.551E-22 | 1.532E-22 | 1.23 | 1.535E-02 |
| Ree29 | 1400.19348 | 3.473E-22 | 3.418E-22 | 1.58 | 1.538E-02 |
| Ree30 | 1402.57259 | 8.790E-23 | 8.365E-23 | 4.84 | 1.588E-02 |
| Ree31 | 1404.94633 | 1.808E-22 | 1.818E-22 | -0.55 | 1.500E-02 |
| Ree32 | 1407.31374 | 4.450E-23 | 4.344E-23 | 2.38 | 1.543E-02 |
| Ree33 | 1409.67516 | 9.342E-23 | 9.219E-23 | 1.32 | 1.524E-02 |
| Ree34 | 1412.02985 | 2.187E-23 | 2.148E-23 | 1.78 | 1.529E-02 |
| Ree35 | 1414.37759 | 4.441E-23 | 4.450E-23 | -0.20 | 1.496E-02 |
| Ree36 | 1416.71806 | 1.016E-23 | 1.012E-23 | 0.39 | 1.502E-02 |
| Ree37 | 1419.05136 | 2.057E-23 | 2.047E-23 | 0.49 | 1.502E-02 |
| Ree38 | 1421.37702 | 4.667E-24 | 4.545E-24 | 2.61 | 1.532E-02 |
| | | | | | |
| Pff35 | 1250.12963 | 1.487E-23 | 1.383E-23 | 6.99 | 1.807E-02 |
| Pff34 | 1252.33119 | 6.076E-23 | 6.024E-23 | 0.86 | 1.695E-02 |
| Pff32 | 1256.71873 | 1.253E-22 | 1.224E-22 | 2.31 | 1.720E-02 |
| Pff30 | 1261.08877 | 2.323E-22 | 2.366E-22 | -1.85 | 1.648E-02 |
| Pff29 | 1263.26912 | 1.072E-22 | 1.076E-22 | -0.37 | 1.672E-02 |
| Pff27 | 1267.62446 | 1.912E-22 | 1.928E-22 | -0.84 | 1.662E-02 |
| Pff26 | 1269.80108 | 7.247E-22 | 7.594E-22 | -4.79 | 1.598E-02 |
| Pff24 | 1274.15638 | 1.220E-21 | 1.259E-21 | -3.20 | 1.620E-02 |
| Pff21 | 1280.70596 | 7.687E-22 | 8.109E-22 | -5.49 | 1.579E-02 |
| Pff19 | 1285.09156 | 1.157E-21 | 1.174E-21 | -1.47 | 1.637E-02 |
| Pff 3 | 1321.25387 | 1.343E-21 | 1.352E-21 | -0.67 | 1.591E-02 |
| Pff 2 | 1323.59436 | 2.393E-21 | 2.359E-21 | 1.42 | 1.620E-02 |
| | | | | | |
| Rff 1 | 1333.05919 | 8.000E-22 | 7.995E-22 | 0.06 | 1.577E-02 |
| Rff19 | 1377.39542 | 1.142E-21 | 1.160E-21 | -1.58 | 1.431E-02 |
| Rff20 | 1379.91348 | 2.900E-21 | 2.895E-21 | 0.17 | 1.448E-02 |
| Rff21 | 1382.43330 | 7.850E-22 | 7.917E-22 | -0.85 | 1.425E-02 |
| Rff22 | 1384.95401 | 1.947E-21 | 1.923E-21 | 1.23 | 1.447E-02 |
| Rff23 | 1387.47488 | 4.949E-22 | 5.117E-22 | -3.39 | 1.374E-02 |
| Rff24 | 1389.99477 | 1.202E-21 | 1.210E-21 | -0.67 | 1.403E-02 |
| Rff25 | 1392.51314 | 3.133E-22 | 3.138E-22 | -0.16 | 1.401E-02 |
| Rff26 | 1395.02890 | 7.160E-22 | 7.225E-22 | -0.91 | 1.382E-02 |
| Rff27 | 1397.54132 | 1.848E-22 | 1.825E-22 | 1.24 | 1.403E-02 |
| Rff28 | 1400.04937 | 4.099E-22 | 4.095E-22 | 0.10 | 1.378E-02 |
| Rff29 | 1402.55207 | 1.089E-22 | 1.008E-22 | 7.44 | 1.477E-02 |
| Rff30 | 1405.04898 | 2.212E-22 | 2.206E-22 | 0.27 | 1.362E-02 |
| Rff31 | 1407.53887 | 5.229E-23 | 5.300E-23 | -1.36 | 1.331E-02 |
| Rff32 | 1410.02106 | 1.118E-22 | 1.131E-22 | -1.16 | 1.324E-02 |
| Rff33 | 1412.49475 | 2.642E-23 | 2.648E-23 | -0.23 | 1.327E-02 |
| Rff34 | 1414.95929 | 5.404E-23 | 5.514E-23 | -2.04 | 1.294E-02 |
| Rff35 | 1417.41389 | 1.266E-23 | 1.259E-23 | 0.55 | 1.318E-02 |
| Rff36 | 1419.85815 | 2.621E-23 | 2.558E-23 | 2.40 | 1.333E-02 |
| Rff37 | 1422.29128 | 5.689E-24 | 5.702E-24 | -0.23 | 1.288E-02 |
| Rff38 | 1424.71292 | 1.110E-23 | 1.130E-23 | -1.80 | 1.258E-02 |

Table 3 (continued)

| Line | Position | $S_{obs}$ | $S_{calc}$ | % | $\|R\|^2_{obs}$ |
|---|---|---|---|---|---|
| Rff39 | 1427.12270 | 2.669E-24 | 2.459E-24 | 7.87 | 1.379E-02 |
| Rff40 | 1429.52048 | 4.608E-24 | 4.757E-24 | -3.23 | 1.221E-02 |
| Rff41 | 1431.90577 | 9.444E-25 | 1.011E-24 | -7.05 | 1.168E-02 |
| Rff42 | 1434.27815 | 1.874E-24 | 1.909E-24 | -1.87 | 1.217E-02 |

[a] The quoted line position is this measured in this work, in $cm^{-1}$. $S_{obs}$ and $S_{calc}$ are measured and calculated intensities, respectively, for pure $^{12}C_2H_2$ (i.e., for a sample containing 100% of $^{12}C_2H_2$), in cm $molecule^{-1}$ at 296 K. % is the ratio $100 \times (S_{obs} - S_{calc}) / S_{obs}$. $|R|^2_{obs}$ is the experimental transition dipole moment squared value, in $D^2$ ($1\ D = 3.33546 \times 10^{-30}$ C m), deduced from $S_{obs}$ using Eqs. (1-3).

Table 4

Line positions and intensities for the forbidden $(\nu_4 + \nu_5)^2$ band of the $^{12}C_2H_2$ molecule in the 7.7 μm region. [a]

| Line | Position | $S_{obs}$ | $\|R\|^2_{obs}$ | $\|R\|^2_{smooth}$ | % |
|---|---|---|---|---|---|
| Pee45 | 1248.78310 | 2.035E-24 | 1.608E-03 | 1.608E-03 | 0.00 |
| Pee42 | 1253.91204 | 2.480E-24 | 1.400E-03 | 1.369E-03 | 2.21 |
| Pee41 | 1255.66410 | 1.084E-23 | 1.289E-03 | 1.289E-03 | 0.00 |
| Pee39 | 1259.23186 | 2.337E-23 | 1.164E-03 | 1.164E-03 | 0.00 |
| Pee36 | 1264.74491 | 2.099E-23 | 9.223E-04 | 9.223E-04 | 0.00 |
| Pee35 | 1266.62567 | 8.859E-23 | 8.838E-04 | 8.730E-04 | 1.22 |
| Pee33 | 1270.45154 | 1.591E-22 | 7.636E-04 | 7.417E-04 | 2.87 |
| Pee32 | 1272.39624 | 6.640E-23 | 6.761E-04 | 6.761E-04 | 0.00 |
| Pee31 | 1274.36192 | 2.715E-22 | 6.605E-04 | 6.046E-04 | 8.46 |
| Pee30 | 1276.34806 | 1.009E-22 | 5.330E-04 | 5.330E-04 | 0.00 |
| Pee29 | 1278.35433 | 4.079E-22 | 5.264E-04 | 4.838E-04 | 8.09 |
| Pee28 | 1280.38115 | 1.728E-22 | 4.973E-04 | 4.346E-04 | 12.61 |
| Pee27 | 1282.42648 | 5.706E-22 | 4.115E-04 | 3.855E-04 | 6.32 |
| Pee25 | 1286.57394 | 6.655E-22 | 2.817E-04 | 2.978E-04 | -5.72 |
| Pee24 | 1288.67440 | 2.612E-22 | 2.593E-04 | 2.593E-04 | 0.00 |
| Pee22 | 1292.92634 | 2.822E-22 | 1.781E-04 | 1.781E-04 | 0.00 |
| Pee20 | 1297.24109 | 3.075E-22 | 1.300E-04 | 1.300E-04 | 0.00 |
| Pee19 | 1299.42044 | 9.323E-22 | 1.100E-04 | 1.100E-04 | 0.00 |
| Pee18 | 1301.61362 | 2.861E-22 | 8.591E-05 | 8.591E-05 | 0.00 |
| Pee17 | 1303.81966 | 8.572E-22 | 7.384E-05 | 7.384E-05 | 0.00 |
| Pee16 | 1306.03816 | 2.538E-22 | 5.734E-05 | 5.734E-05 | 0.00 |
| Pee15 | 1308.26857 | 6.702E-22 | 4.471E-05 | 4.471E-05 | 0.00 |
| Pee14 | 1310.51011 | 1.807E-22 | 3.265E-05 | 3.265E-05 | 0.00 |
| Pee13 | 1312.76231 | 5.009E-22 | 2.760E-05 | 2.760E-05 | 0.00 |
| Pee12 | 1315.02439 | 1.216E-22 | 1.879E-05 | 1.879E-05 | 0.00 |
| Pee11 | 1317.29587 | 2.607E-22 | 1.272E-05 | 1.272E-05 | 0.00 |
| Pee 9 | 1321.86562 | 1.309E-22 | 6.117E-06 | 6.117E-06 | 0.00 |
| Pee 8 | 1324.16302 | 2.630E-23 | 3.733E-06 | 3.733E-06 | 0.00 |
| Pee 7 | 1326.46831 | 4.587E-23 | 2.261E-06 | 2.261E-06 | 0.00 |
| Pee 6 | 1328.78108 | 7.072E-24 | 1.123E-06 | 1.123E-06 | 0.00 |
| Pee 5 | 1331.10092 | 1.105E-23 | 6.514E-07 | 6.514E-07 | 0.00 |
| Pee 4 | 1333.42772 | 8.858E-25 | 1.855E-07 | 1.855E-07 | 0.00 |
| Qfe 5 | 1342.89810 | 5.326E-24 | 2.844E-07 | 3.146E-07 | -10.62 |
| Qfe 7 | 1342.98093 | 1.283E-23 | 5.811E-07 | 5.865E-07 | -0.93 |
| Qfe 9 | 1343.08942 | 2.207E-23 | 9.620E-07 | 9.439E-07 | 1.88 |
| Qfe10 | 1343.15298 | 7.978E-24 | 1.057E-06 | 1.155E-06 | -9.24 |
| Qfe11 | 1343.22331 | 3.069E-23 | 1.404E-06 | 1.387E-06 | 1.23 |
| Qfe12 | 1343.29997 | 1.062E-23 | 1.534E-06 | 1.640E-06 | -6.93 |
| Qfe13 | 1343.38257 | 3.806E-23 | 1.974E-06 | 1.915E-06 | 2.98 |
| Qfe14 | 1343.47178 | 1.379E-23 | 2.344E-06 | 2.211E-06 | 5.65 |
| Qfe15 | 1343.56714 | 4.082E-23 | 2.565E-06 | 2.529E-06 | 1.40 |
| Qfe18 | 1343.89142 | 1.305E-23 | 3.707E-06 | 3.610E-06 | 2.61 |
| Qfe20 | 1344.13921 | 1.127E-23 | 4.505E-06 | 4.438E-06 | 1.49 |
| Qfe21 | 1344.27247 | 3.092E-23 | 4.977E-06 | 4.884E-06 | 1.87 |
| Qfe22 | 1344.41219 | 8.953E-24 | 5.312E-06 | 5.351E-06 | -0.74 |
| Qfe27 | 1345.20371 | 1.164E-23 | 7.821E-06 | 8.008E-06 | -2.39 |
| Qfe28 | 1345.38070 | 3.017E-24 | 8.113E-06 | 8.604E-06 | -6.05 |

Table 4 (continued)

| Line | Position | $S_{obs}$ | $\|R\|^2_{obs}$ | $\|R\|^2_{smooth}$ | % |
|---|---|---|---|---|---|
| Qfe29 | 1345.56395 | 7.464E-24 | 8.984E-06 | 9.220E-06 | -2.63 |
| Qfe30 | 1345.75320 | 2.096E-24 | 1.033E-05 | 9.859E-06 | 4.56 |
| Qfe31 | 1345.98592 | 4.739E-24 | 1.072E-05 | 1.052E-05 | 1.88 |
| Ree 6 | 1359.45680 | 4.732E-24 | 6.294E-07 | 6.294E-07 | 0.00 |
| Ree 7 | 1361.86361 | 3.411E-23 | 1.431E-06 | 1.431E-06 | 0.00 |
| Ree 8 | 1364.27775 | 1.961E-23 | 2.399E-06 | 2.399E-06 | 0.00 |
| Ree10 | 1369.13001 | 4.938E-23 | 6.127E-06 | 6.127E-06 | 0.00 |
| Ree11 | 1371.56944 | 2.074E-22 | 8.880E-06 | 8.880E-06 | 0.00 |
| Ree12 | 1374.01690 | 9.446E-23 | 1.285E-05 | 1.285E-05 | 0.00 |
| Ree13 | 1376.47437 | 3.649E-22 | 1.780E-05 | 1.780E-05 | 0.00 |
| Ree14 | 1378.94166 | 1.486E-22 | 2.383E-05 | 2.383E-05 | 0.00 |
| Ree16 | 1383.90889 | 2.037E-22 | 4.088E-05 | 4.088E-05 | 0.00 |
| Ree17 | 1386.40773 | 6.574E-22 | 5.025E-05 | 5.025E-05 | 0.00 |
| Ree18 | 1388.92278 | 2.463E-22 | 6.557E-05 | 6.557E-05 | 0.00 |
| Ree19 | 1391.44885 | 7.775E-22 | 8.144E-05 | 8.144E-05 | 0.00 |
| Ree20 | 1393.98831 | 2.600E-22 | 9.755E-05 | 9.755E-05 | 0.00 |
| Ree21 | 1396.54189 | 7.762E-22 | 1.175E-04 | 1.175E-04 | 0.00 |
| Ree22 | 1399.11015 | 2.496E-22 | 1.394E-04 | 1.394E-04 | 0.00 |
| Ree23 | 1401.69371 | 7.102E-22 | 1.642E-04 | 1.642E-04 | 0.00 |
| Ree24 | 1404.29302 | 2.156E-22 | 1.889E-04 | 1.889E-04 | 0.00 |
| Ree25 | 1406.90872 | 5.911E-22 | 2.200E-04 | 2.200E-04 | 0.00 |
| Ree26 | 1409.54126 | 1.733E-22 | 2.498E-04 | 2.498E-04 | 0.00 |
| Ree27 | 1412.19099 | 4.534E-22 | 2.856E-04 | 2.856E-04 | 0.00 |
| Ree28 | 1414.85824 | 1.250E-22 | 3.137E-04 | 3.137E-04 | 0.00 |
| Ree29 | 1417.54325 | 3.080E-22 | 3.461E-04 | 3.461E-04 | 0.00 |
| Ree30 | 1420.24715 | 8.452E-23 | 3.874E-04 | 3.874E-04 | 0.00 |
| Ree32 | 1425.70969 | 5.366E-23 | 4.727E-04 | 4.727E-04 | 0.00 |
| Ree33 | 1428.46892 | 1.250E-22 | 5.177E-04 | 5.177E-04 | 0.00 |
| Ree34 | 1431.24710 | 3.097E-23 | 5.502E-04 | 5.502E-04 | 0.00 |
| Ree35 | 1434.04395 | 6.952E-23 | 5.946E-04 | 5.946E-04 | 0.00 |
| Ree36 | 1436.85956 | 1.694E-23 | 6.349E-04 | 6.349E-04 | 0.00 |
| Ree37 | 1439.69380 | 3.707E-23 | 6.882E-04 | 6.882E-04 | 0.00 |
| Ree38 | 1442.54669 | 8.757E-24 | 7.309E-04 | 7.309E-04 | 0.00 |
| Ree39 | 1445.41781 | 1.812E-23 | 7.638E-04 | 7.638E-04 | 0.00 |
| Ree40 | 1448.30716 | 4.153E-24 | 8.067E-04 | 8.067E-04 | 0.00 |
| Ree41 | 1451.21437 | 8.433E-24 | 8.487E-04 | 8.487E-04 | 0.00 |

[a] The quoted line position is this measured in this work, in $cm^{-1}$. $S_{obs}$ is the measured intensity for pure $^{12}C_2H_2$ (i.e., for a sample containing 100% of $^{12}C_2H_2$), in cm $molecule^{-1}$ at 296 K. $|R|^2_{obs}$ is the experimental transition dipole moment squared value deduced from $S_{obs}$ using Eqs. (1-4), and $|R|^2_{smooth}$ its smoothed value, in $D^2$ (1 D = $3.33546 \times 10^{-30}$ C m). % is the ratio $100 \times (|R|^2_{obs} - |R|^2_{smooth}) / |R|^2_{obs}$. Except for the *Q*-branch, this ratio should not be understood as an observed – calculated residual. When non zero, it means that the experimental value has been changed to set up the line list, and indicates how much.

Table 5

Summary of $^{12}C_2H_2$ experimental vibrational transition dipole moments squared $|R_0|^2$ in $D^2$ (1 D = 3.33546 × $10^{-30}$ C m), and Herman-Wallis coefficients, see Eqs. (2-8), in the 7.7 μm spectral region [a]

| Band | Origin | $\|R_0\|^2$ | | $A_1^{PR}$ | $A_2^{PR}$ |
|---|---|---|---|---|---|
| $(2\nu_4 + 2\nu_5)^0_- - (\nu_4 + \nu_5)^2$ | 1311.308 | $3.15(57)\times10^{-7}$ [b] | | $-5.377(460)\times10^{-2}$ | $+8.377(1700)\times10^{-4}$ |
| $(\nu_4 + 2\nu_5)^1$ II $- \nu_5^1$ | 1318.730 | $1.673(12)\times10^{-2}$ | *e* | $-6.9(18)\times10^{-4}$ | $-1.19(70)\times10^{-5}$ |
| | | | *f* | $-1.71(16)\times10^{-3}$ | |
| $(2\nu_4 + 2\nu_5)^2$ II $- (\nu_4 + \nu_5)^0_-$ | | 1320.908 | | Impossible to adjust with Herman-Wallis factors | |
| $(\nu_4 + \nu_5)^0_+$ | 1328.081 | $6.030(73)\times10^{-3}$ [c] | | $-9.2(11)\times10^{-4}$ | $-6.12(56)\times10^{-5}$ |
| $(2\nu_4 + \nu_5)^1$ II $- \nu_4^1$ | 1328.314 | $1.587(14)\times10^{-2}$ | *e* | $-7.8(17)\times10^{-4}$ | |
| | | | *f* | $-1.67(19)\times10^{-3}$ | $-2.40(69)\times10^{-5}$ |
| $(\nu_4 + \nu_5)^2$ | 1342.821 | Impossible to adjust with Herman-Wallis factors | | | |
| $(2\nu_4 + \nu_5)^1$ I $- \nu_4^1$ | 1348.006 | $1.268(42)\times10^{-4}$ | *e* | $+3.5(27)\times10^{-3}$ | $-2.29(23)\times10^{-3}$ |
| | | | *f* | $-6.11(72)\times10^{-3}$ | $+9.91(74)\times10^{-4}$ |
| $(2\nu_4 + \nu_5)^3 - \nu_4^1$ | 1350.273 | Impossible to adjust with Herman-Wallis factors | | | |

[a] 95% confidence intervals (2 SD, in unit of the last quoted digit) are given between parenthesis. For $|R_0|^2$ values, the overall accuracy is 5%, except for the $(2\nu_4 + 2\nu_5)^0_- - (\nu_4 + \nu_5)^2$ band for which it is estimated to be at least 20%. Non given Herman-Wallis coefficients have been fixed at zero.

[b] For this band, $|R_0|^2$, $A_1^{PR}$ and $A_2^{PR}$ have a poor physical meaning. Excess digits in $A_1^{PR}$ and $A_2^{PR}$ are non significant but necessary to reproduce the experimental data (see Section 3). Note that Eq. (8) has been used for this forbidden band, contrary to the allowed bands for which Eq. (7) has been used.

[c] $|R_0|^2 = 5.8229\times10^{-3}$ $D^2$ in Ref. [9], strictly speaking, not comparable with our value since obtained from a different theoretical model.

Table 6

Summary of new bands and transitions available for the $^{12}C_2H_2$ molecule at 7.7 µm [a]

| Band | Origin | $\nu_{min}$ - $\nu_{max}$ | $\Sigma S$ | $S_{min}$ - $S_{max}$ | $J_{max}\nu/J_{max}S/J_{max}$ | | | Cd$\nu$ | Cd$S$ |
|---|---|---|---|---|---|---|---|---|---|
| 000220–_–000112 | 1311.31 | 1288-1377 | 1.9E-21 | 1.0E-25-6.4E-22 | 13-23 | [b] -23 | 13-23 | 4/2 | 5/3 |
| 000121_2–000011 | 1318.73 | 1225-1423 | 2.1E-19 | 1.0E-24-5.5E-21 | 37-38 | 37-38 | 40-40 | 4/3 | 6/5 |
| 000222_2–000110– | 1320.91 | 1246-1403 | 1.2E-21 | 3.4E-25-7.4E-23 | 33-32 | 33-32 | 33-32 | 4/3 | 6/4 |
| 000110+_–000000+ | 1328.08 | 1224-1449 | 2.7E-18 | 1.5E-25-1.4E-19 | 43-45 | 43-45 | 45-50 | 4/3 | 7/5 |
| 000211_2–000101 | 1328.31 | 1224-1442 | 3.6E-19 | 1.5E-25-9.4E-21 | 39-42 | 37-42 | 45-45 | 4/3 | 6/5 |
| 000112__–000000+ | 1342.82 | 1248-1452 | 1.8E-20 | 2.1E-25-9.1E-22 | 45-41 | 45-41 | 45-41 | 4/3 | 6/5 |
| | | | | | 31 | 31 | 31 | 4/3 | 6/5 |
| 000211_1–000101 | 1348.01 | 1288-1420 | 2.7E-21 | 1.8E-24-9.1E-23 | 22-26 | 20-23 | 25-30 | 4/3 | 6/5 |
| 000213__–000101 | 1350.27 | 1277-1421 | 9.4E-22 | 2.8E-24-4.8E-23 | 32-28 | 32-28 | 32-28 | 4/2 | 6/4 |

[a] Explanation of the column headings:

Band: vibrational assignment used in the line list, according to Section 1: $v_1$ $v_2$ $v_3$ $v_4$ $v_5$ $\ell \pm r$ for the upper and lower states. When ± or *r* does not occur for the upper state, it is replaced by an underscore. Note that *r* is mentionned only if necessary to avoid ambiguities.

Origin: approximate value of the band center, in $cm^{-1}$.

$\nu_{min}$ - $\nu_{max}$ : limiting values of line positions, in $cm^{-1}$.

$\Sigma S$ : sum of line intensities, in cm $molecule^{-1}$ at 296 K.

$S_{min}$ - $S_{max}$ : limiting values of line intensities, in cm $molecule^{-1}$ at 296 K.

$J_{max}\nu$ : maximum value of *J* for which a line position has been measured.

$J_{max}S$ : maximum value of *J* for which a line intensity has been measured.

$J_{max}$ : maximum value of *J* present in the line list.

(The first value is for the *P*-branch and the second for the *R*-branch. When a value is on a separate line, it concerns the *Q*-branch of the above band.)

Cd$\nu$: uncertainty code for line positions [17]. Code 2: $10^{-2}$-$10^{-1}$ $cm^{-1}$. Code 3: $10^{-3}$-$10^{-2}$ $cm^{-1}$. Code 4: $10^{-4}$-$10^{-3}$ $cm^{-1}$.

Cd*S*: uncertainty code for line intensities [17]. Code 4: 10-20%. Code 5: 5-10%. Code 6: 2-5%. Code 7: 1-2%.

(The second value is for some interpolated or extrapolated lines.)

Other spectroscopic data are the same as those already put in the last updates of the databases: air- and self-broadening coefficients, default value for the temperature exponent of air-broadening coefficients, constant value for the air-pressure shifting coefficient, and their accuracies [17,28].

[b] No intensity measurement in the *P*-branch of this band.

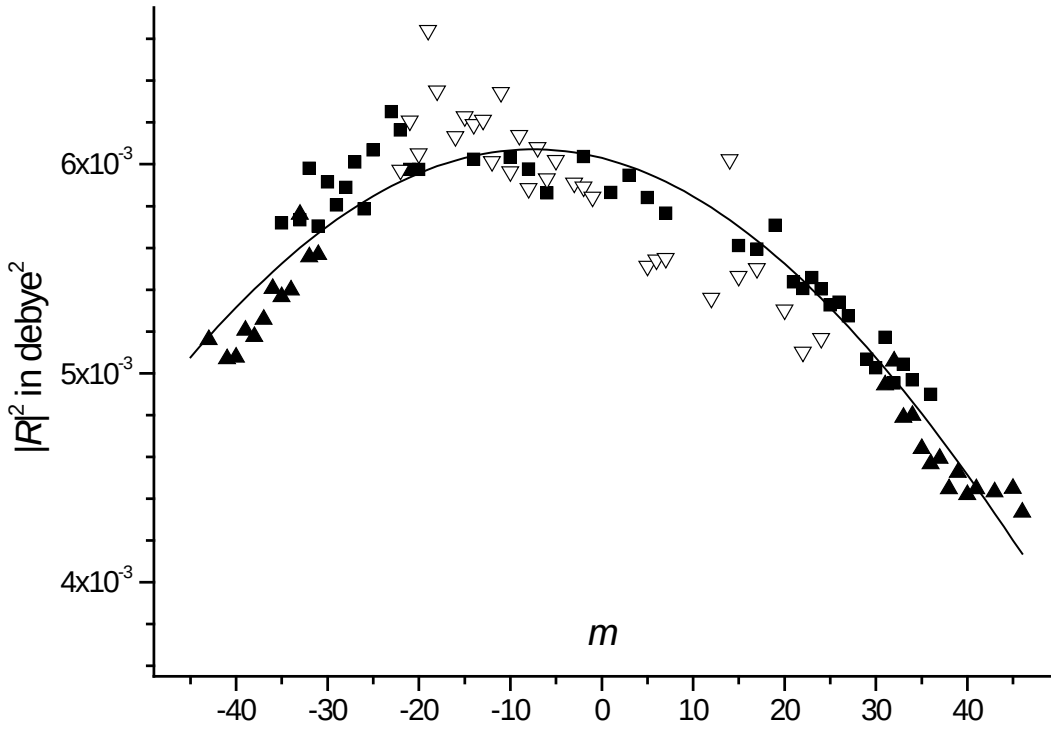


Fig. 1. Variation of the transition dipole moment squared $|R|^2$, in $D^2$ (1 D = 3.33546 × $10^{-30}$ C m), vs. *m*, for the $(\nu_4 + \nu_5)^0_+$ band. Solid triangles are experimental values obtained in this work. Solid squares are experimental values deduced from intensities measured by Vander Auwera [9] (when several values, coming from different spectra, are given for a line in Ref. [9], they have been averaged). Open triangles are experimental values deduced from intensities measured by Lepère et al [11]. (Experimental intensities quoted in Refs. [9,11] were preliminarily converted for a sample of 100% of $^{12}C_2H_2$.) The solid line represents the values calculated using the constants reported in Table 5. They result from an unweighted fit including the experimental data of this work and those of Vander Auwera [9] (see Section 3).

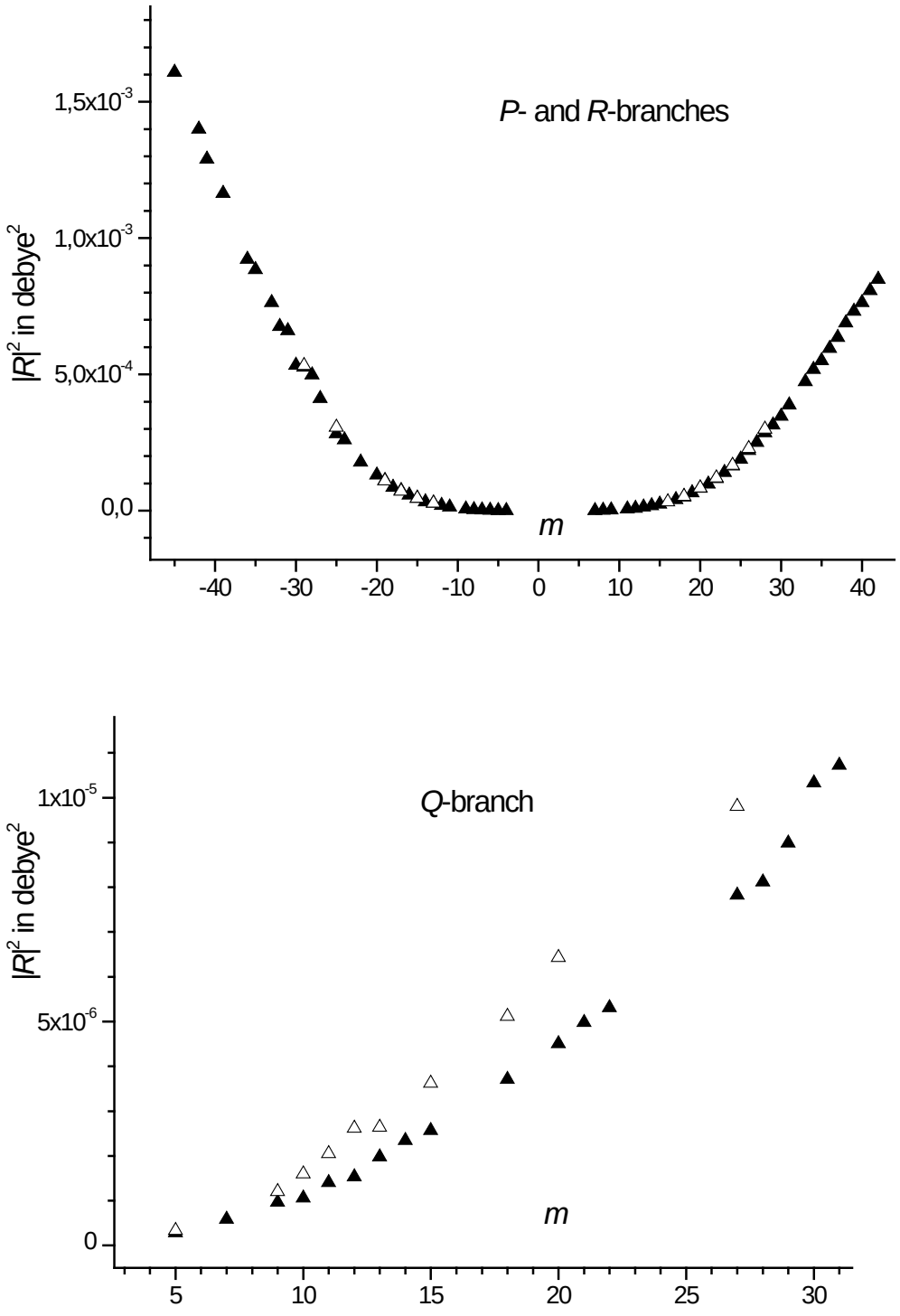


Fig. 2. Variation of the transition dipole moment squared $|R|^2$, in $D^2$ (1 D = 3.33546 × $10^{-30}$ C m), vs. *m*, for the $(\nu_4 + \nu_5)^2$ band. Solid triangles are experimental values obtained in this work. Open triangles are experimental values deduced from intensities measured by Vander Auwera [9]. The upper plot shows *P*-and *R*-branches whereas the lower plot shows the *Q*-branch.

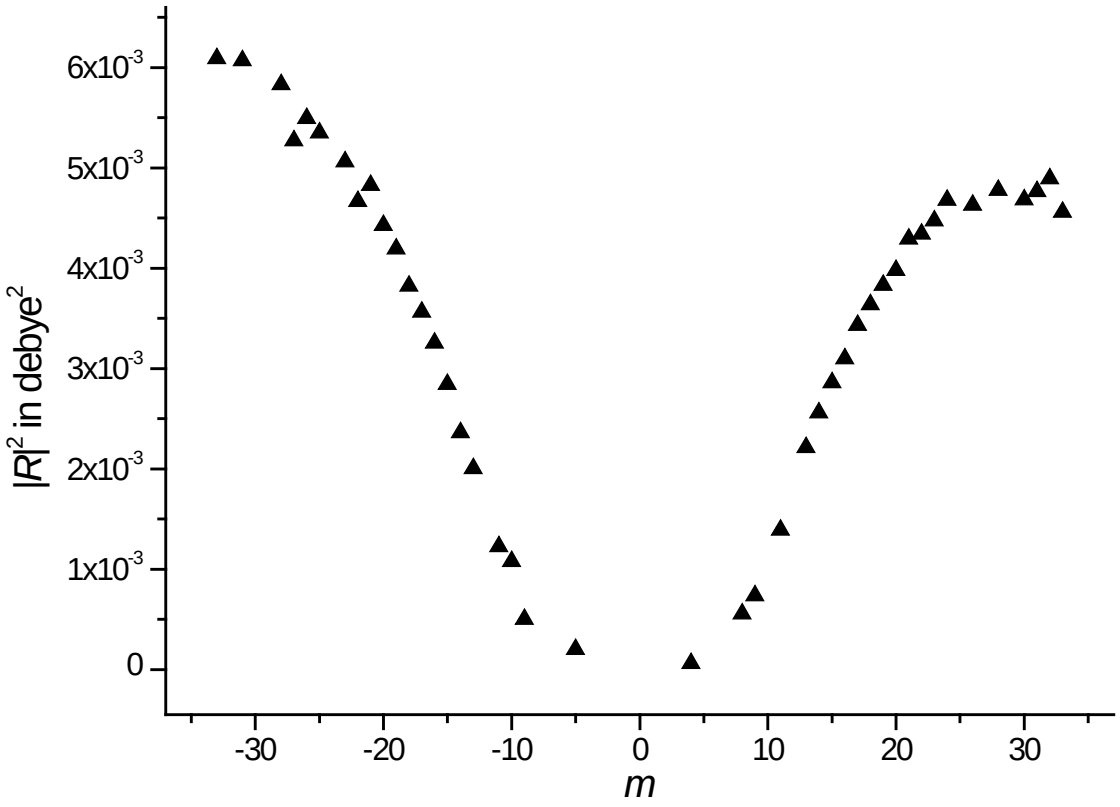


Fig. 3. Variation of the transition dipole moment squared $|R|^2$, in $D^2$ (1 D = 3.33546 × $10^{-30}$ C m), vs. *m*, for the $(2\nu_4 + 2\nu_5)^2$ II – $(\nu_4 + \nu_5)^0_-$ band. Solid triangles are experimental values obtained in this work.

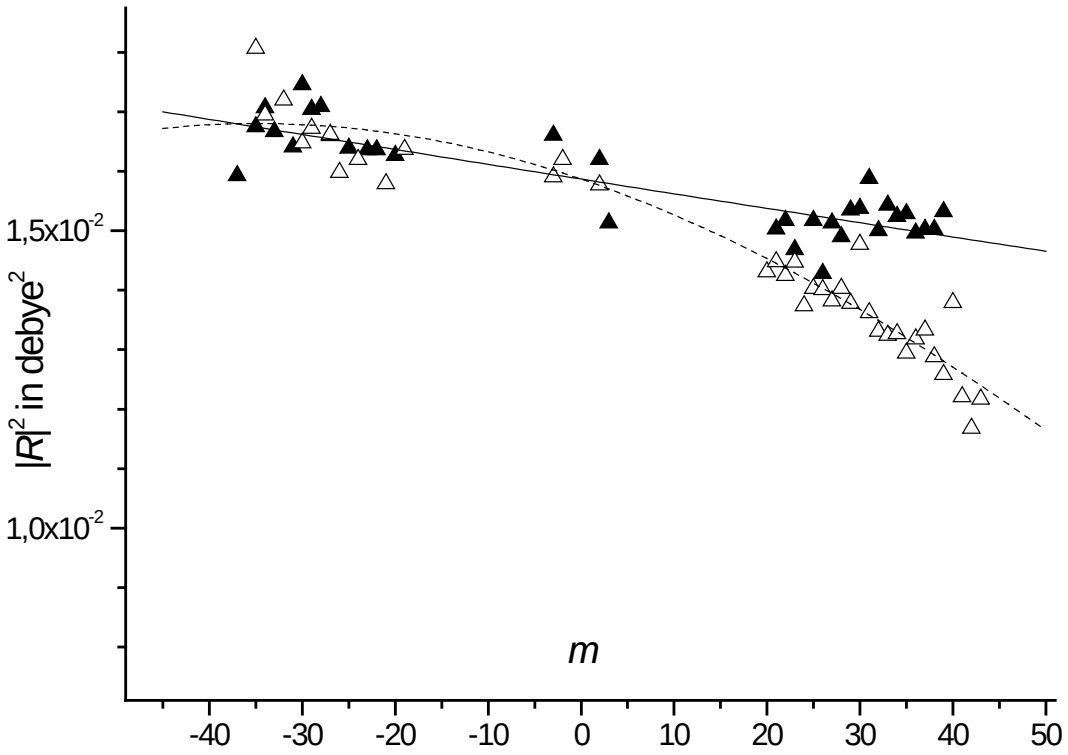


Fig. 4. Variation of the transition dipole moment squared $|R|^2$, in $D^2$ (1 D = 3.33546 × $10^{-30}$ C m), vs. *m*, for the $(2\nu_4 + \nu_5)^1\,\Pi - \nu_4{}^1$ band. Solid triangles are experimental values obtained in the *e* sub-band, and open ones in the *f* sub-band. The lines represent the values calculated using the constants reported in Table 5. The solid line is for the *e* sub-band, and the dashed one for the *f* sub-band.

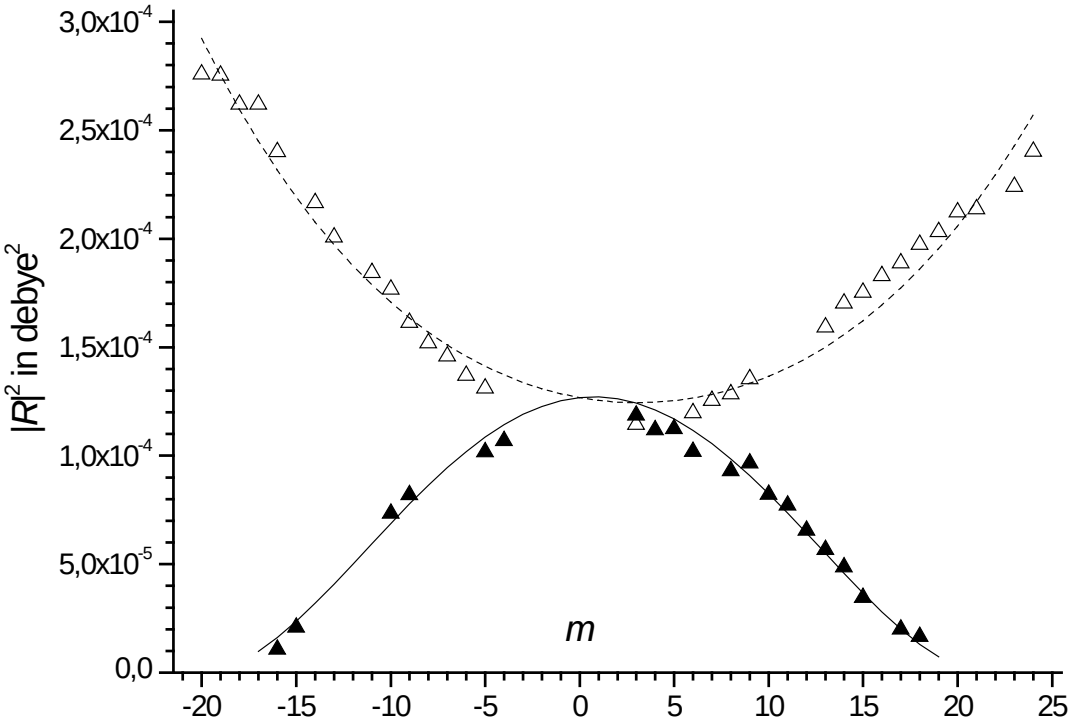


Fig. 5. Variation of the transition dipole moment squared $|R|^2$, vs. $m$, for the $(2\nu_4 + \nu_5)^1$ I – $\nu_4{}^1$ band. See caption of Fig. 4.